Melting of the Shallow Upper Mantle: A New Perspective

Article *in* Journal of Petrology · August 1991

DOI: 10.1093/petrology/32.4.671

1 author:

Dimitrios Kostopoulos
National and Kapodistrian University of Athens
76 PUBLICATIONS **2,116** CITATIONS

SEE PROFILE

0022-3530/91 $3.00

Melting of the Shallow Upper Mantle: A New Perspective

by DIMITRIS K. KOSTOPOULOS

Department of Geological Sciences, University of Durham, Science Laboratories, South Road, Durham DH1 3LE, UK

(*Received 14 June 1989; revised typescript accepted 14 November 1990*)

ABSTRACT

Detailed examination of liquidus phase relationships in binary and ternary joins of the CFMAS + Cr system has permitted a rigorous determination of the dry melting path of an initially fertile spinel peridotite composition resembling Bulk Silicate Earth or MORB–pyrolite. It is demonstrated that it is impossible to model mantle melting accurately using only one set of ratios of phases entering the melt; this implies that the melting process is primarily controlled by solid solution rather than eutectic behaviour. The proportions of phases entering a melt depend on whether a phase reacts and/or disappears from a system, and on the choice of the initial and final peridotite compositions. Four discrete domains in the melting regime of upper-mantle peridotites are distinguished, each characterized by different phase melting coefficients, relating to the melting of: (1) lherzolites, (2) clinopyroxene-bearing harzburgites (i.e., free-clinopyroxene), (3) clinopyroxene-saturated harzburgites (i.e., clinopyroxene in solid solution in orthopyroxene), and (4) clinopyroxene-free harzburgites (i.e., no clinopyroxene). The proposed non-linear fashion in which mantle lithologies melt explains the inadequacy of all previous models to reproduce the observed compositions of upper-mantle peridotite melting residues. It is suggested that: (1) olivine and orthopyroxene will melt cotectically; (2) clinopyroxene and spinel will lose most of their aluminous component after ~8% melting within the first 4 kb (~12 km) of ascent from the dry solidus; and that (3) clinopyroxene will disappear completely from a MORB–pyrolite mantle after ~42% melting. Although such a number is significantly higher than that dictated by the position of the clinopyroxene-out curves from peridotite isobaric equilibrium melting experiments (~22%), it is emphasized that the latter are a gross oversimplification of the natural melting process and are not equivalent to melting during adiabatic upwelling. It is concluded that the commonly postulated disappearance of clinopyroxene from fertile peridotite compositions at ~22% melting is greatly in error if melting in an adiabatically rising mantle is considered, thus providing an explanation for many unsuccessful attempts by various authors to model the behaviour of transition elements in sub-oceanic and supra-subduction-zone mantle and derivative magmas.

INTRODUCTION

Uncertainties in the mantle composition and melting regime

Mantle composition and melting form the cornerstone of magma genesis. Mantle composition refers to the mode and bulk-rock chemistry, whereas mantle melting refers to the proportions in which various phases enter the melt (hereafter melting or melt contribution coefficients). Table 1 is a compilation from the literature of modes and melting models previously proposed for fertile spinel lherzolites. It is apparent that, for any single phase, a very wide range of modal abundances and melt contribution coefficients has been suggested by various workers. In brief, modal abundances and melt contribution coefficients summarized from the data tabulated in Table 1 span the ranges $Ol_{42-70}Opx_{18-32}$-$Cpx_{8-26}Sp_{0-5}$ and $Ol_{42-35}Opx_{8-60}Cpx_{40-73}Sp_{5-30}$ respectively. [Abbreviations: Ol = olivine; Opx = orthopyroxene; Cpx = clinopyroxene; Sp = spinel; Fo = forsterite; Fa = fayalite; Di = diopside; En = Enstatite; Pig = Pigeonite; Liq = liquid.] Such spectra of

TABLE 1

Compositions and melting proportions (wt.%) of fertile spinel lherzolites

Source composition				Melting proportions				
Ol	*Opx*	*Cpx*	*Sp*	*Ol*	*Opx*	*Cpx*	*Sp*	*Reference*
0·60	0·20	0·20		0·25	0·08	0·67		Pearce & Norry (1979); Furnes *et al.* (1987)
0·42	0·27	0·26	0·05	−0·424	0·539	0·731	0·154	Carter (1970); Presnall *et al.* (1979);
0·51	0·21	0·23	0·05	−0·424	0·539	0·731	0·154	Ottonello *et al.* (1984); Bonatti *et al.* (1986);
0·42	0·27	0·26	0·05	−0·416	0·530	0·743	0·143	Brophy & Marsh (1986)
0·509	0·217	0·230	0·044	−0·18	0·41	0·67	0·10	Lin *et al.* (1989)
0·55	0·20	0·20	0·05	0·15	0·15	0·40	0·30	Beccaluva *et al.* (1984)
0·60	0·20	0·16	0·04	0.15	0·15	0·40	0·30	(sequential melting scheme)
0·65	0·20	0·12	0·03	0.25	0·10	0·65		
0·46	0·32	0·20	0·02		0·43	0·45	0·12	Viereck *et al.* (1989)
0·58	0·29	0·13		0·25	0·20	0·55		
0·60	0·25	0·15		0·25	0·20	0·55		Condie (1985)
0·59	0·28	0·13		0·20	0·20	0·60		Stosch *et al.* (1986); Roden *et al.* (1988)
0·55	0·25	0·20		0·20	0·20	0·60		Frey (1984)
0·60	0·20	0·20		0·20	0·20	0·60		Lippard *et al.* (1986); Thompson *et al.* (1984)
0·65	0·20	0·15		0·10	0·30	0·60		Michael (1988)
0·65	0·22	0·13		0·29	0·22	0·49		Navon & Stolper (1987)
0·65	0·20	0·15		0·15	0·25	0·60		Leeman (1976)
0·51	0·21	0·23	0·05	0·10	0·20	0·60	0·10	
0·625	0·229	0·146		0·25	0·25	0·50		Wood (1978)
0·50	0·25	0·25		0·15	0·35	0·50		Wood (1979)
0·58	0·18	0·24		−0·08	0·54	0·54		Frey *et al.* (1985)
0·54	0·27	0·14	0·05	0·22	0·23	0·45	0·10	Vukadinovic & Nicholls (1989)
0·60	0·25	0·15		0·20	0·25	0·55		White & Schilling (1978)
0·60	0·25	0·15		0·25	0·25	0·50		Walker (1984)
0·49	0·30	0·21		0·35	0·25	0·40		Dupuy *et al.* (1987)
0·53	0·31	0·16		0·35	0·25	0·40		
0·58	0·20	0·20	0·02	−0.25	0·56	0·69		Furnes *et al.* (1986*a*)
				or	0·45	0·55		
				— 0·30 —		0·70		Klein & Langmuir (1987)
					0·30	0·70		Prinzhofer & Allègre (1985)
					0·375	0·515	0·110	Sinigoi *et al.* (1980) (10% melt)
					0·345	0·566	0·089	(20% melt)
0·55	0·25	0·15	0·05	0·10	0·30	0·55	0·05	Ewart & Hawkesworth (1987)
				−0·67	1·00	0·67		Bodinier (1988)
				or	0·60	0·40		

variations, with values for individual phases differing by well over 100%, illustrate very clearly the uncertainties involved when estimating mantle modal mineralogies and melting coefficients, and must be resolved.

A detailed evaluation of the modal and chemical composition of undepleted spinel lherzolites has been presented by Kostopoulos & James (submitted). These authors, who discussed at length the mineralogical, geochemical, and cosmochemical criteria for mantle fertility, concluded that the Primitive Upper Mantle (PUM) or Bulk Silicate Earth (BSE) would have been relatively homogeneous and would have had an average modal composition $Ol_{57}Opx_{25\cdot5}Cpx_{15}Sp_{2\cdot5}$, hereafter fertile spinel lherzolite or FSL (maximum errors on modal abundances of individual phases are: Ol: 1·75%; Opx: 3·92%; Cpx: 6·67%; Sp: 20%). As far as the proportions of minerals and the concentrations of compatible elements in the mantle source are concerned, MORB–pyrolite or Depleted MORB Mantle (DMM) would also be represented by FSL (Kostopoulos & James, submitted).

With regard to the melting scheme of the mantle source, Table 1 shows that, in spite of the existing variability, there is a general agreement that Cpx is the major contributor to the melt (~60–70 wt.%); Opx comes second in importance, whereas Ol and Sp play only a minor role. The negative contribution of Ol to the melt implies construction of this phase upon fusion (i.e., an incongruent melting relationship with Opx), and is discussed in more detail below. It will be noted, however, that in most petrogenetic models there is no justification for the values of the melting coefficients employed, whereas in others melting coefficients have been established by trace-element inversion (see Table 1 for references). In this respect it is necessary to emphasize that melting coefficients should not only be capable of reproducing the observed melt compositions (i.e., trace element patterns) but also reproduce the observed residual compositions and be based on experimental phase relations. Inasmuch as most lavas represent pooled melts, that is, compositions integrated over a specific, non-linear, melting interval during isentropic upwelling of asthenosphere [see Klein & Langmuir (1987), McKenzie & Bickle (1988), and Kostopoulos & James (submitted) for details and mathematical formulation], inversion techniques cannot be used to infer melting coefficients. Another *ad hoc* assumption, made in almost all petrogenetic models, in trying to establish melting coefficients, is that mantle melting is governed by a uniform regime; that is, it can be described by a single set of ratios of phases entering the melt. This method certainly simplifies calculations but has the disadvantage of not considering phase disappearance, phase reaction, and/or solid-solution phenomena that occur during melting.

Although our understanding of mantle melting is still imperfect, it is possible to constrain the compositional paths of melts and residues using published analyses of basalts and peridotites from individual sites, simple mass-balance equations and phase-equilibria arguments. Melting of spinel peridotites can be rigorously examined in the CMAS system with the aid of the Fo–SiO_2, Di–En, and Di–Fo binary joins, the Di–Fo–SiO_2 ternary projection, and additional sections involving Fe, Cr, and H_2O. Perhaps an appropriate starting point would be to evaluate the negative contribution of olivine to the melt; this approach is employed by many workers in their calculations.

MANTLE MELTING IN PERIDOTITE-BOUNDING BINARY JOINS

Melting of enstatite

The basis for using a negative contribution of olivine to the melt in petrogenetic modelling (Table 1) is the peritectic reaction relation of En to Fo+Liq, discovered by Bowen & Andersen (1914) (Fig. 1a). With respect to the incongruent dissolution of En, however,

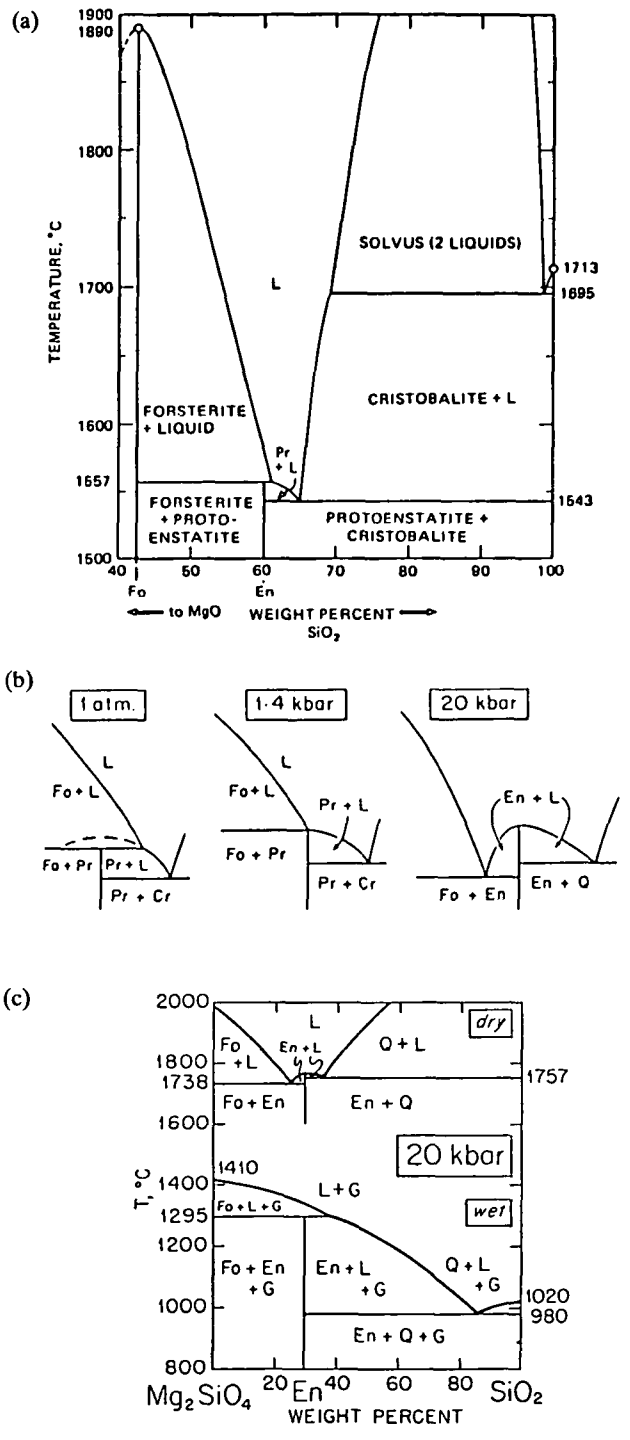

FIG. 1. (a) One-atm temperature–composition diagram for the join Fo–SiO_2. (b) Schematic isobaric temperature–composition sections showing the change from incongruent to congruent melting of protoenstatite. (c) Dry and wet melting relations of enstatite at 20 kb. Dry diagram at top is an isobaric temperature–composition section. Wet diagram is a projection from H_2O. G: Gas (from Morse, 1980).

attention is drawn to the fact that, in the absence of H_2O, it is restricted to pressures lower than ~2·3 kb (Boyd *et al.*, 1964), and most probably it occurs at $P < 1{\cdot}4$ kb (Morse, 1980) (Fig. 1b). Such low pressures will apply only to the top parts of melting diapirs which, having lost most of their basaltic component during ascent, are not likely to contribute >1% to the total (i.e., pooled) melt produced (Kostopoulos & James, submitted). Excess H_2O will greatly enhance the incongruent melting behaviour of En even at high pressures (Kushiro *et al.*, 1968) (Fig. 1c) and in the presence of other CMS components (Kushiro, 1969) (see Fig. 6 below), but conditions of H_2O-saturation (i.e., $P_{H_2O} = P_{load}$) at the source regions of basic magmas are the exception rather than the rule in nature.

Michael & Chase (1987) and Michael (1988) have calculated that peridotites parental to MORB lavas contain ~0·01–0·045 wt.% H_2O. This suggests that melting beneath spreading ridges takes place under essentially anhydrous conditions. Further, H_2O behaves in an incompatible manner similar to that of Nd (Michael, 1988) and hence will be efficiently extracted from the mantle with the first melt fraction. H_2O is a more significant ingredient in the mantle in supra-subduction zone (SSZ) environments. However, primitive SSZ lavas, for which experimental evidence is clearly in favour of a 'peritectic' origin (e.g., Cape Vogel type boninites; Van der Laan *et al.*, 1989), have H_2O contents of only ~2 wt.% (Kyser *et al.*, 1986; Dobson & O'Neil, 1987) and are H_2O-undersaturated at pressures >2 kb (e.g., $a_{H_2O} \sim 0{\cdot}4$ at 10 kb; Walker & Cameron, 1983). Thus, with the exception of low-Ca boninites and certain deep-seated, Si-undersaturated alkali-mafic rocks, the shape of the liquidus phase surfaces of which is largely regulated by volatiles [see recent reviews by Eggler (1987) and Wyllie (1987, 1988) and references therein], magma genesis in the shallow upper mantle (i.e., Sp lherzolite facies) will be dominated by congruent melting of En. Moreover, the presence of Fe in solid solution in natural Ol and Opx argues strongly against the incongruent melting behaviour of En even at low pressures in dry systems. Figure 2a shows the atmospheric phase relations in the system Fo–An–SiO_2, whereas Fig. 2b shows the atmospheric phase relations in the same system with the important difference that Fo has been replaced by Ol of composition $Fo_{51}Fa_{49}$. Clearly, Fe addition to the pure CMAS system (e.g., ~12 wt.% FeO at R; Fig. 2b) has the very significant effect of converting the melting path of mantle peridotites from peritectic into eutectic (at least, at low pressures).

Melting of forsterite

The congruent melting of En in the mantle discussed above requires that the melting coefficient of Ol should be at least nought (or greater). Mantle olivines show a limited, yet perceptible variation in Fo (e.g., Fo_{89-92}) that correlates positively and smoothly with melting indices (Carter, 1970; Jaques & Green, 1980; Michael & Bonatti, 1985; Arai, 1987), which is too great a magnitude to have been acquired solely via subsolidus exchange (as is clearly evident from experimentally calibrated thermobarometers involving Ol and any of the phases Opx, Cpx, and Sp). Olivine therefore has to melt, and will melt in a cotectic (with En) fashion for most of its life in the mantle. Reference to Fig. 6 (below) shows that under anhydrous conditions at 20 kb, melts in equilibrium with Fo and mutually saturated Di and Pig (point V) are composed of $Di_{61}En_{28}Fo_{12}$ (5·1:2·3:1), whereas liquids in equilibrium with Fo and mutually saturated Pig and En (point U) are composed of $Di_{58}En_{33}Fo_9$ (6·4:3·7:1). As pressure drops, these ternary eutectic points will move away from Fo, implying that, during isentropic ascent of asthenospheric material that intersected its dry solidus at 20 kb (maximum solidus intersection pressure for most MORB and arc magmas; Nicholls & Ringwood, 1972, 1973; Nicholls, 1974; Green, 1976; Duncan & Green, 1987; Falloon & Green, 1988; Falloon *et al.*, 1988), Ol will contribute <10% to the melt.

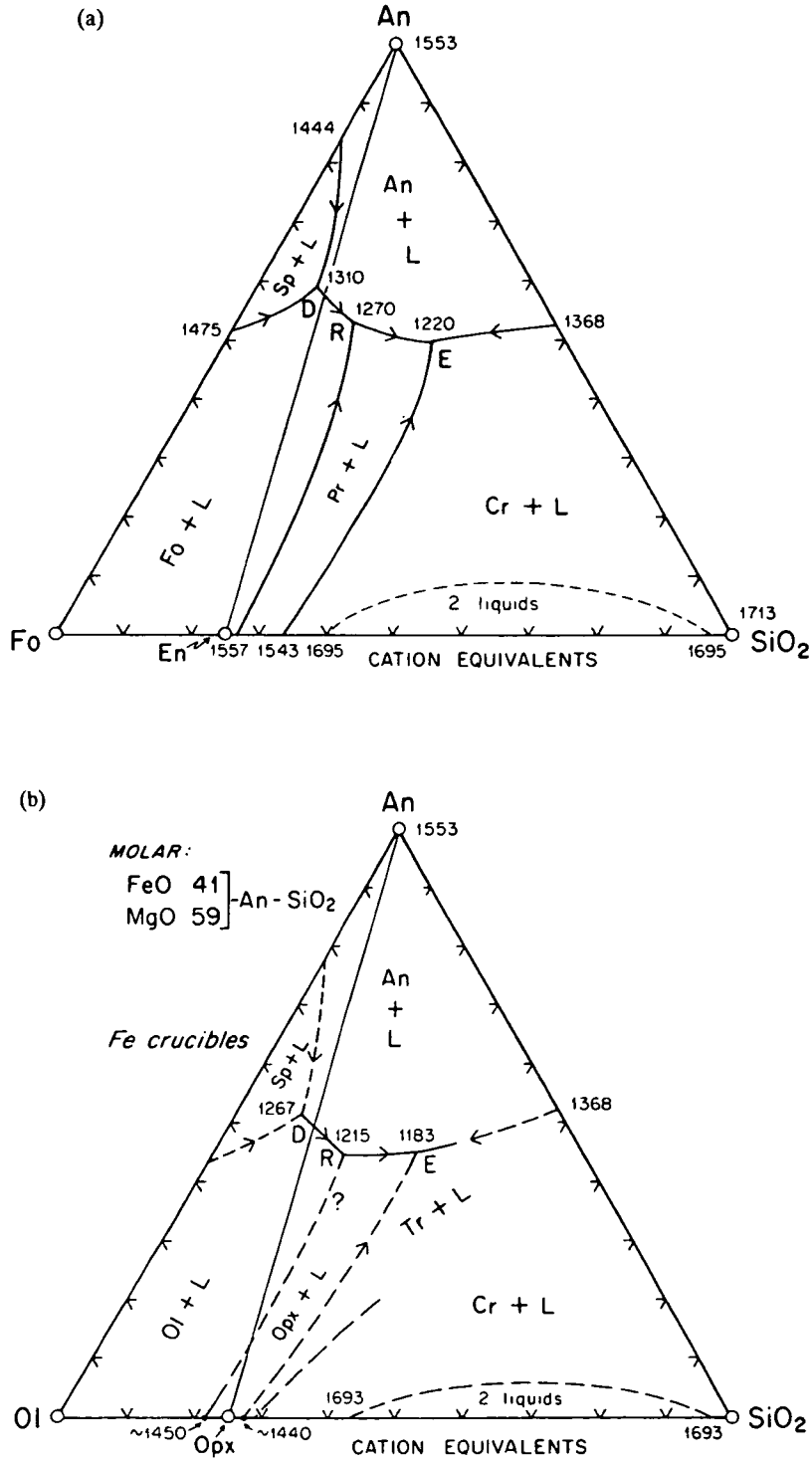

FIG. 2. One-atm liquidus relations in the systems (a) Fo–An–SiO_2 and (b) Ol–An–SiO_2 for a molar ratio MgO:FeO = 59:41. [Note the marked effect of Fe addition to the pure CMAS system on the disappearance of the incongruent melting behaviour of En even at low pressures (from Morse, 1980).]

Additional support for this comes from the Fo–Fa loop (Fig. 3). MORB–pyrolite olivine is tightly constrained near Fo_{89}; lherzolite/harzburgite transitional lithologies (i.e., modal Cpx ~ 5 wt.%) contain ~Fo_{90} whereas harzburgites with traces of Cpx (i.e., ~0·5 wt.%) contain ~Fo_{92} [see references cited earlier and Green *et al.* (1979), Brown (1982), Augé (1983), Roberts (1986), Takahashi (1986), and Elthon (1989)]. Figure 3a dictates that during initial melting of a MORB-source peridotite in the lherzolite facies ($Fo_{89} \rightarrow Fo_{90}$) olivine will contribute ~3% to the melt whereupon, in the harzburgite facies ($Fo_{90} \rightarrow Fo_{92}$), it will contribute ~9% (additional) melt until fusion stops. According to this figure, the *mg*-numbers (i.e., $100 \times Mg/[Mg + Fe^{2+}]$) of the liquids in equilibrium with Fo_{90}, Fo_{91}, and Fo_{92} are ~64·6, 66·7, and 69·5 respectively, which lie well within the range of (near-)primary magmas, allowing perhaps for minor (~5 wt.%) olivine fractionation. Green *et al.* (1979) reasoned that 24% equilibrium melting of MORB–pyrolite (*mg*-number = 90·1) at 20 kb yields primary MORB (*mg*-number = 69·5) in equilibrium with Cpx-free harzburgite (*mg*-number = 91·6), in excellent agreement with the Fo and *mg*-number values obtained from the Fo–Fa system. The advantage of the latter is that it supplies information about the amount of olivine that will actually melt. The shape of the olivine loop remains unchanged at high pressures (Fig. 3b), which suggests that the mineral will always be contributing small amounts to the melt.

Phase relations in the Mg_2SiO_4–SiO_2 system (Chen & Presnall, 1975; fig. 1) show that at 12 kb, Fo–En mixtures (i.e., cpx-free harzburgites) will melt at a eutectic: $Fo_{13}En_{87}$ [the mirror image of that used by Brophy & Marsh (1986)]. The effect of pressure on this eutectic is negligible: $Fo_{21}En_{79}$ at 25 kb (Chen & Presnall, 1975), $Fo_{16}En_{84}$ at 30 kb, and $Fo_{27}En_{73}$ at 70 kb (Kato & Kumazawa, 1985). Careful inspection of Fig. 6 also reveals that the additional presence of Cpx in the mantle will barely affect the position of the Fo–En eutectic. It appears therefore that an 'internal melting ratio': Opx:Ol = 6·7:1 (hereafter Cpx-free harzburgite eutectic), can safely be used throughout the pressure melting range of spinel (and garnet) peridotite lithologies.

Melting of diopside

Phase relations along the Di–En join (Fig. 4a) are somewhat complicated because of the presence of Pig and miscibility gaps between En and Di, for a wide temperature interval on both sides of the Di solidus at pressures up to 15 kb (Huebner, 1980; Carlson, 1988; Carlson & Lindsley, 1988). Mantle peridotites do not contain Pig; instead, they have En-rich Opx and Di-rich Cpx in equilibrium. This discrepancy is due to the additional presence of Fe, Ti, Na, Al, and Cr in the natural system, as compared with pure CMS compositions, which act to suppress the Di–En liquidus relations below the Pig stability field (Lindsley & Andersen, 1983; Davidson & Lindsley, 1985). However, the CMS system can still be used with confidence, provided that Pig is carefully dealt with. In Fig. 4a, point P represents an En–Di mixture in MORB–pyrolite proportions (~2:1). Upon heating at 1 atm, this assemblage will convert into a Pig–Di mixture (~3:1) which, eventually, will melt to Fo + Liq. The pseudo-eutectic liquid is located at R and will not leave this point until all Di is consumed. Liquid R is composed of ~$Di_{69}En_{39}$.

In the dry Di–Fo system at 1 atm and 20 kb, pseudo-eutectic liquid compositions are located at about $Di_{88}Fo_{12}$ and $Di_{76}Fo_{24}$ respectively (Figs. 4b and 6). In the presence of silica (i.e., system Di–Fo–SiO_2) under identical conditions, liquids in equilibrium with Fo and mutually saturated Di and Pig have compositions near $Di_{69}Fo_{19}SiO_{2_{12}}$ and $Di_{61}Fo_{31}SiO_{2_8}$ respectively (points R and V; Fig. 6), whereas liquids in equilibrium with Fo and mutually saturated Pig and En lie at approximately $Di_{57}Fo_{27}SiO_{2_{16}}$ and

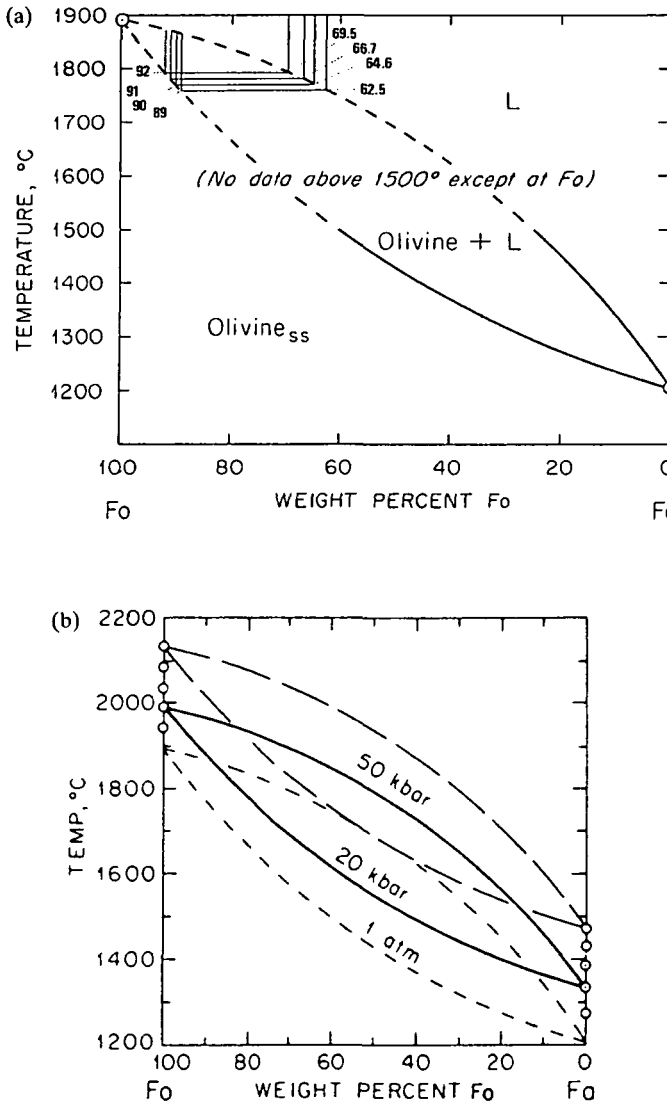

FIG. 3. Melting of Ol (a) at 1 atm and (b) at higher pressures (from Morse, 1980). The compositions of mantle Ol (expressed as %Fo) and their equilibrium liquids (expressed as *mg*-number) are shown for the 1-atm diagram.

$Di_{58}Fo_{32}SiO_{2_{10}}$ respectively (points Q and U; Fig. 6). Addition of excess H_2O at 20 kb shifts point V towards SiO_2, but still Di contributes some 50% to the ternary melt ($Di_{50}Fo_{31}SiO_{2_{19}}$, point W; Fig. 6). Therefore, melts in equilibrium with dry spinel lherzolite at pressures < 20 kb would contain a minimum of 50%, and more likely $\sim$65% Di component.

Another method of calculating the amount of Cpx entering the liquid during melting of spinel lherzolites involves the solution of mass-balance equations for Sm, Yb, or Sc concentrations in MORB lavas, for which the degree of melting has been determined independently [e.g., experimentally, or from major elements; see Klein & Langmuir (1987)]. Sm, Yb, and Sc are preferred principally for three reasons. First, they are moderately incompatible during melting of spinel lherzolite assemblages, hence their abundances in a

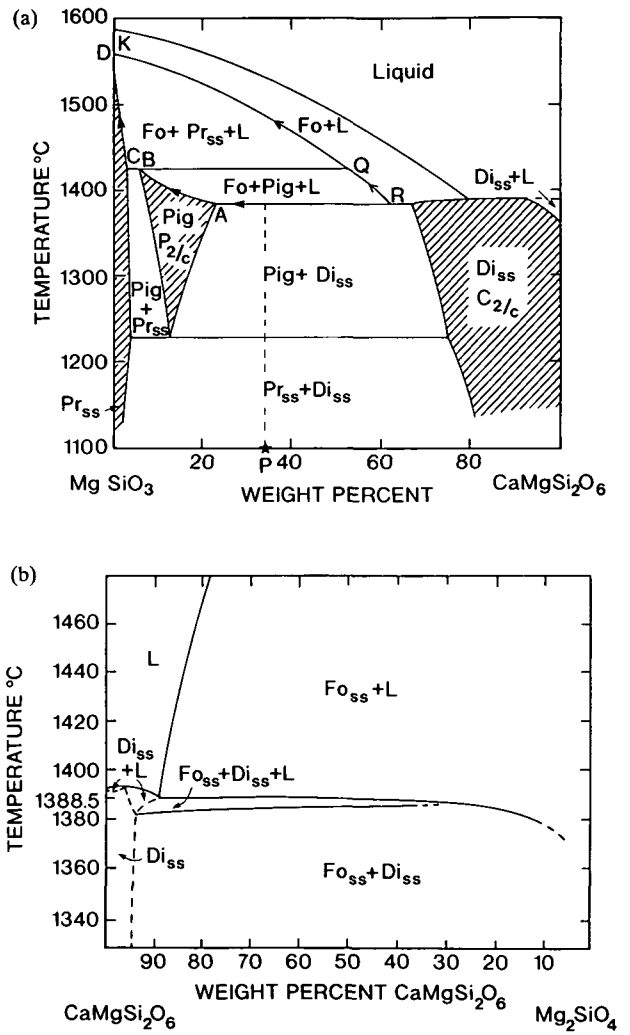

FIG. 4. One-atm temperature–composition diagrams for the joins (a) En–Di and (b) Di–Fo. In (a), the shaded areas are fields of homogeneous single pyroxene separated by solvi (from Morse, 1980). Equilibrium melting of bulk composition P produces a series of residues A–B–C–D (filled arrowheads) and a series of liquids R–Q–K (open arrowheads). (For a full explanation, see text and Fig. 6.)

MORB source should approximate those in the primitive upper mantle. Second, they are unlikely to be substantially modified by processes such as mantle metasomatism or removal of small melt fractions. Third, in spinel lherzolites, they are hosted almost exclusively in Cpx. The equation for non-modal equilibrium partial melting of mantle peridotite (Shaw, 1970) is

$$C_L = C_o/[D_o + F(1-P)] \quad (1)$$

where C_o is the abundance of any element in the source, C_L is its concentration in the magma, D_o is the bulk distribution coefficient at the onset of melting, F is the degree of melting, and P is the distribution coefficient for the actual portion of the solid that is being converted into liquid. Rearranging (1) gives

$$P = [C_L(D_o + F) - C_o]/(C_L F). \quad (2)$$

Assuming that P is constant, then for any two extents of melting, F_1 and F_2, (2) gives

$$P=[C_{L1}D_o+C_{L1}F_1-C_o)/(C_{L1}F_1) \quad (3)$$

and

$$P=[C_{L2}D_o+C_{L2}F_2-C_o)/(C_{L2}F_2). \quad (4)$$

Eliminating P from (3) and (4) leads to

$$D_o=[C_o(C_{L2}F_2-C_{L1}F_1)]/[C_{L1}C_{L2}(F_2-F_1)]. \quad (5)$$

Viereck *et al.* (1989) have shown by means of least-squares mass balances that low-Ti (N1) and high-Ti (N2) MORB can be derived by ~14–16 and 8–10% melting respectively of fertile spinel lherzolite [see also Klein & Langmuir (1987) and Kostopoulos & James (submitted)]. According to these authors, average N1-MORB contains 2·22 ppm Sm whereas average N2-MORB contains 3·17 ppm Sm. The concentration of Sm in MORB–pyrolite is 0·358 ppm (Kostopoulos & James, submitted). Substitution of the above variables in (5) yields $D_o=0{\cdot}0404\pm0{\cdot}0080$. When the appropriate D_o and F_1 or F_2 values are substituted in either (3) or (4), they yield $P=0{\cdot}1945$. The distribution coefficient of Sm between Cpx and liquid under mantle melting conditions is very well constrained experimentally to lie between 0·24 and 0·28 (Grutzeck *et al.*, 1974; Nakamura *et al.*, 1982; Green & Pearson, 1985; McKay *et al.*, 1986), suggesting that $\sim75\pm7\%$ Cpx is required to enter the liquid to satisfy the derived P value.

Melting of spinel

Melting of spinel is somewhat more difficult to treat as this phase does not appear on any of the joins discussed so far. In the CMAS tetrahedron, stoichiometric spinel occurs on the MgO–Al_2O_3 edge (Fig. 5a), remote from the sub-tetrahedron of interest, Fo–Di–An–SiO_2 (Fig. 5b). This awkward positioning of spinel does not allow application of the lever rule to estimate the proportion of the mineral in the melt, despite the presence of its liquidus surface across the Fo–An join. Melting of pure Mg–Al spinel is none the less of little importance as it applies only to the initial stages of melting of MORB–pyrolite. Jaques & Green (1980) have explicitly documented that during melting of undepleted spinel lherzolite, the initial Mg–Al spinel melts within 25–30 °C of the dry solidus by solid solution change to refractory Cr spinel which persists to pressures as low as 1 atm. Spinel *cr*-number (i.e., $100\times Cr/[Cr+Al]$) ranges from ~8 in primitive spinel lherzolite to ~80 in extremely residual harzburgite and correlates positively with olivine *mg*-number (Arai, 1987), testifying to a continuous melting regime in the upper mantle (Dick & Bullen, 1984). Phase relations in the Di-rich part of the $CaMgSi_2O_6$–$MgCr_2O_4$ (Di-picrochromite) join at 1 atm (Fig. 5c; Onuma & Tohara, 1983), suggest the existence of a binary pseudo-eutectic at ~1·3 wt.% chromite, implying that the refractory Cr-spinel in the mantle will contribute only minimal amounts to the melt. The latter observation is generally attested to by the large liquidus volume of $MgCr_2O_4$ in systems containing this mineral in equilibrium with other mantle silicates (Arculus *et al.*, 1974; Arculus & Osborn, 1975; Muan, 1975; Irvine, 1977; Onuma & Tohara, 1983; Irvine & Sharpe, 1986).

Dickey *et al.* (1971) and Onuma & Tohara (1983) have shown that Di containing >0·9–1 wt.% Cr_2O_3 will melt incongruently to Cr-Sp + Liq (see Fig. 5c). Clinopyroxenes from FSL lithologies contain a maximum 0·7 wt.% Cr_2O_3 (see references cited earlier in the Fo section); therefore, no incongruent melting of Cpx will occur during the early stages of melting. Clinopyroxenes from Sp harzburgite lithologies contain a maximum 1·2 wt.%

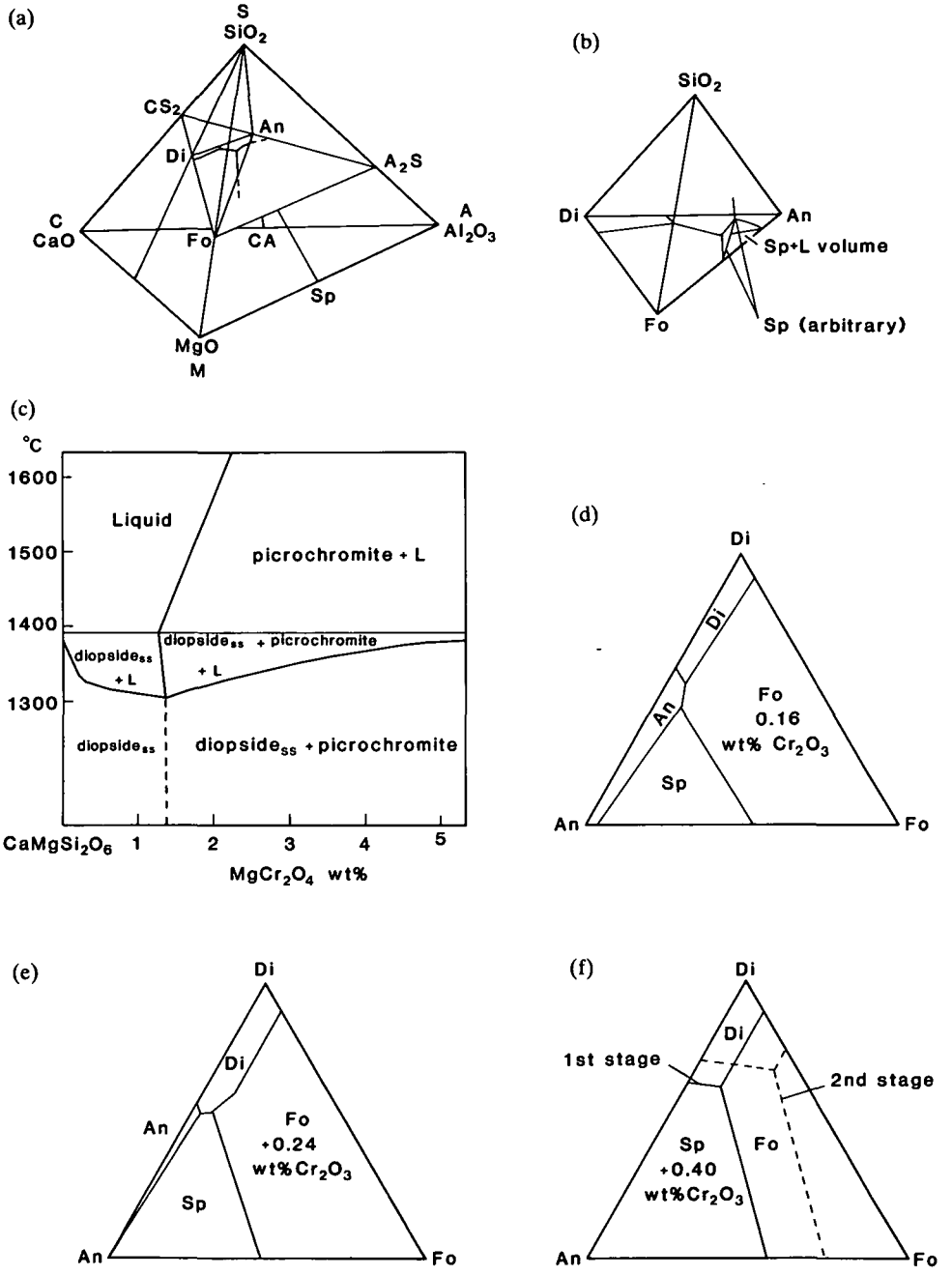

FIG. 5. Position of the sub-tetrahedron Di–Fo–An–SiO_2 (a) in the CMAS tetrahedron and (b) its relation to the liquidus volume of Sp (from Morse, 1980); (c) liquidus relations in the system Di–Pc (from Onuma & Tohara, 1983); liquidus phase relations in the system Di–Fo–An–Pc with (d) 0·16 wt.% Cr_2O_3, (e) 0·24 wt.% Cr_2O_3, (f) 0·4 wt.% Cr_2O_3 (from Onuma & Tohara, 1983); first- and second-stage eutectics refer to melting of MORB–pyrolite and more depleted lherzolite/harzburgite in equilibrium with Al-rich (i.e., *cr*-number <40) and Cr-rich (i.e., *cr*-number >40) Sp respectively.

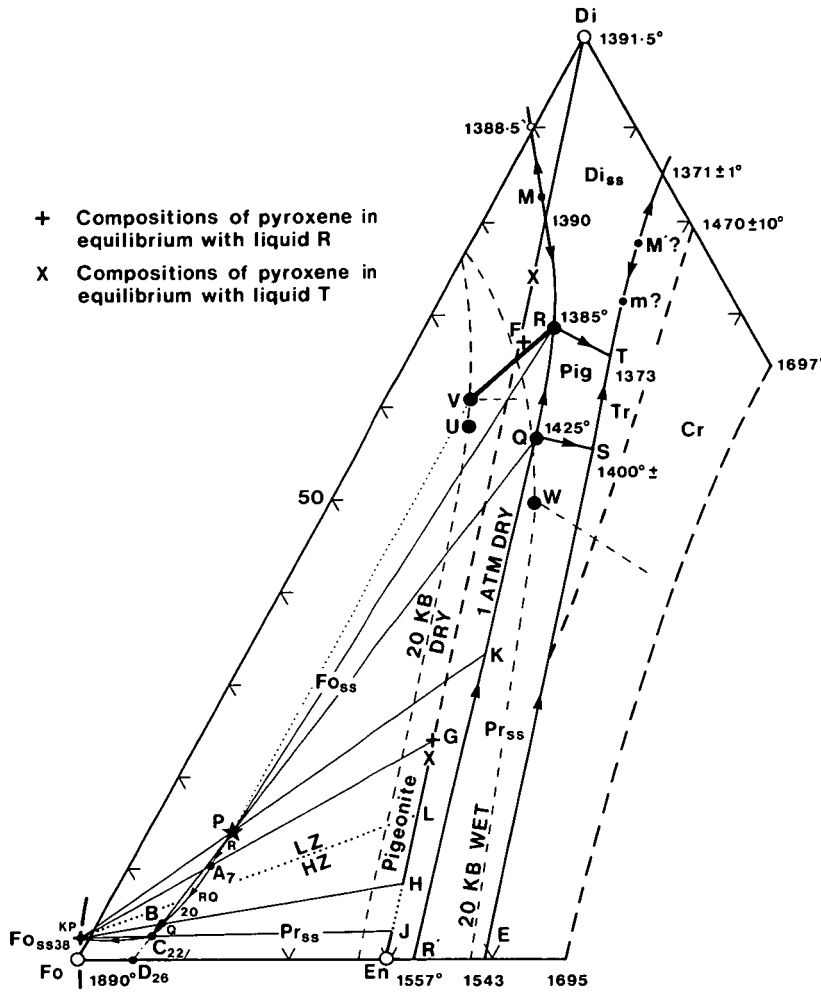

FIG. 6. Phase equilibrium diagram for the system Fo–Di–SiO_2 (a) at 1 atm dry (from Morse, 1980) and (b) at 20 kb, both dry and wet (from Kushiro, 1969). Equilibrium melting of a model MORB–pyrolite composition (Point P: $Fo_{59}En_{27}Di_{14}$) is discussed in the text. Points A, B, C, D, and Fo (large capital letters) represent successive residues of melting, and subscripts indicate the degree of total melting (measuring from P). Small filled arrowheads mark the compositional path of the solid, and the small capital letters next to them denote the corresponding path of the liquid (for each segment of the melting path). Thick dots represent the lherzolite/harzburgite boundary (at 5 wt.% modal Cpx). (Note that the liquid path RQR′ is peritectic at 1 atm but not at pressures > 5 kb dry.) Abbreviations: ss: solid solution; Di: diopside; En: enstatite; Fo: forsterite; Pr: protoenstatite; Cr: cristobalite; Tr: tridymite.

Cr_2O_3 (references as above) and may melt incongruently, but the small amount of Cpx in harzburgites, coupled with the position of the Di–Pc pseudo-eutectic (Fig. 5c), suggests that the effect of incongruent melting of Cpx on the composition of the liquid will be unnoticeable.

Onuma (1983) and Onuma & Tohara (1983) have shown that addition of Cr to the Di–Fo–An plane suppresses the liquidus volume of anorthite below this plane. Their experimental results for variable addition of Cr are summarized as Figs. 5d–f. Of interest here is the section containing 0·4 wt.% Cr_2O_3 (Fig. 5f) as it closely resembles the Earth's upper mantle [see Kostopoulos & James (submitted) and references therein]. Nevertheless,

Figs. 5d and e serve to illustrate the rapid decline in the proportion of spinel entering the melt as it becomes increasingly Cr-rich with advanced melting, thus further corroborating the arguments given above [see also Sinigoi *et al.* (1980)]. In Fig. 5f, the ternary 'pseudo-eutectic' lies at about $Di_{61}Fo_{12}Sp_{27}$, in good agreement with the previous estimates of the proportions of Di and Fo in the liquid.

It should be clarified that this 'pseudo-eutectic' liquid composition relates only to the initial stages of melting of MORB–pyrolite, and for this reason it is labelled 'first stage'. In reality, mantle melting is thought to involve buoyancy-driven segregation of melts from a deformable matrix, with the melt separating rapidly in upwelling regions, being $<3\%$ anywhere at a particular time within the mantle (McKenzie, 1984, 1985; Ribe, 1985, 1988). This means that progressive melt extraction in ascending diapirs will also be accompanied by melting of progressively Cr-richer sources, making the eutectic point of Fig. 5f move away from the spinel corner. The exact path to be followed is not known, but an approximate position, where the transformation of spinel from predominantly Al-rich to predominantly Cr-rich will be accomplished, can be drawn with relatively small error, based on phase diagrams involving pure picrochromite (see references cited earlier). This is shown schematically in Fig. 5f (dashed line) and is labelled 'second stage'. Once spinel becomes sufficiently Cr-rich (e.g., Cr-number ~ 40) no other significant shift of the ternary eutectic is expected to occur.

In view of the preceding discussion, a simplified two-stage melting of spinel can be envisaged. During first-stage melting of fertile MORB–source peridotite, spinel will be predominantly (Mg–Al)-bearing, entering the melt in a ratio to Cpx of $\sim 1{:}4$. During second-stage melting, spinel will be predominantly Cr-bearing, entering the melt in a ratio to Cpx of $\sim 1{:}12$ (Fig. 5f). No higher resolution than this is possible at present with the available amount of data. Synoptically, the weight contribution of various phases to the melt during melting of fertile spinel lherzolite, as constrained by experimental petrology, will approximately be $Ol_{0-5}Opx_{5-15}Cpx_{60-80}Sp_{10-20}$.

Preliminary inferences on the melting regime of spinel lherzolites

Supra-solidus isentropic rise of asthenosphere is a polybaric, polythermal path with a negative slope of $\sim 7\,^{\circ}C/kb$ (see McKenzie, 1984). Along this path, the melting regime of spinel peridotites will be largely controlled by the decreasing solubility of Cpx in Opx and the progressively more refractory nature of spinel. With respect to the former, unmixing of aluminous Opx with falling pressure (see Duncan & Green, 1987) will tend to prevent the residual mantle mineralogy from escaping from the four-phase field Ol + Opx + Cpx + Sp. The net result of this would be the persistence of Cpx in the mantle at extents of melting larger than those suggested by the Cpx-out curve for any given pressure. During the initial stages of melting of MORB–pyrolite when the melt fraction is small and the source is Cpx-rich, exsolution of Cpx will not appreciably affect the ratio of the various minerals entering the liquid as predicted by phase equilibria. With advanced melting at lower pressures, however, the phase diagrams, being isobaric equilibrium sections, will miss the shift of the two-pyroxene solvus and, consequently, will induce an error in the calculated degree of melting and phase melting proportions. Because of the high Ol/Cpx and Opx/Cpx ratios in refractory peridotites, the error will be correspondingly small for Ol and Opx but critical for Cpx.

The situation can be conceived as one of melting bouncing to and fro between Ol + Opx + Cpx and Ol + Opx eutectics, depending on the initial temperature on the solidus and the ascent rate of the mantle diapir, as well as the initial abundance and composition of Opx and

its rate of unmixing. To these complexities should be added the progressively smaller proportion of spinel entering the melt with increasing degree of melting (as outlined above). Careful treatment of pyroxene and spinel is crucial if rigorous petrogenetic modelling involving the transition elements is to be made, and is examined in the ensuing paragraphs.

It was remarked in the Di melting section that pyroxene phase relations in the CMS system predict existence of a Pig component between Di and En (Fig. 4a). However, this is in profound contrast to the naturally coexisting En-rich Opx and Di-rich Cpx observed in peridotites. This intermediate Pig component reflects the limits of mutual solubility of the two pyroxenes mentioned earlier, i.e., it may be viewed as a fictive solvus, with the En + Pig field belonging to En at high pressures and passing to Di at lower pressures. Such being the case, compositions of four-phase peridotites (i.e., Ol + Opx + Cpx + Sp) will project, at higher pressures, into the Fo-saturated part of the Fo + Di + Pig and Fo + Pig areas of Fig. 6 (triangle FFoH); by contrast, compositions of three-phase peridotites containing Cpx-saturated Opx will project into the Fo-saturated part of the Fo + Pig + En and Fo + En areas (triangle HFoEn), whereas pure three-phase peridotites (i.e., Ol + Opx + Sp) will project onto the Fo–En join [at low pressures, the Fo-saturated part of the Fo–Pig–En area (triangle HFoJ) is removed from the Cpx-saturated three-phase field and attached to the four-phase field]. On this basis, harzburgites (i.e., mantle rocks with <5 wt.% modal Cpx) can be classified as Cpx-bearing (LFoH), Cpx-saturated (HFoEn), and Cpx-free (Fo-En). This terminology will be employed henceforth.

Dick & Fisher (1984) and Dick *et al.* (1984) presented a simplified sketch of the Di–Fo–En system at $P>10$ kb, which is portrayed in Fig. 7. It is very clear that their Ol + Opx + Cpx + Sp and Ol + Opx + Sp fields (Fig. 7b) correspond to the (higher-pressure) FFoH and HFoEn areas of Fig. 6 explained above. Also shown in Fig. 7a is the Ol–Opx–Cpx modal ternary diagram with the compositions of abyssal peridotites from various localities. Strictly speaking, the modal diagram corresponds to the four-phase field in the sketch but, because most Cpx-bearing harzburgites with low absolute Cpx content represent re-equilibrated Cpx-saturated rocks, it may include the (lower three-phase) Ol–Opx–Sp field as well.

Another important point to make here is that the transition from lherzolite to harzburgite lithologies will occur somewhere along the Pig solidus (curve AB, Fig. 4a). The approximate position of this boundary is shown in Fig. 6 as line FoL (thickly dotted). Inspection of Fig. 4a also reveals that the En solidus and the En–(En + Pig) solvus have very steep slopes. This suggests that for melting in the four-phase field, the amount of Di dissolved in En will be nearly constant until all free Di melts out, and that the Di-out point will act as a thermal barrier to melting, with extra heat requirements needed for fusion to proceed beyond this point. Once this divide is breached, the Di content of En is no longer constrained by the solvus and decreases steadily with further melting. Diapiric ascent would none the less ensure that the Di content of En would be solvus-constrained for most of the length of the adiabatic path, progressively diminishing as shallower depths are approached.

MANTLE MELTING IN PERIDOTITE-BOUNDING TERNARY JOINS

Having discussed phase relations in peridotite-bounding binary joins, melting in the Di–Fo–SiO_2 ternary system can now be examined. For the sake of simplicity, only the equilibrium case will be considered which, for Fo-rich compositions, approximates that for fractional melting (Morse, 1980). According to Fig. 6, in the pressure range 20 kb–1 atm under anhydrous conditions, partial melting of MORB–pyrolite (point P: $Fo_{59}En_{27}Di_{14}$) will release a series of initial liquids lying along VR (thick solid line). As explained earlier, point V is eutectic (Fo + Di + Pig = Liq), whereas R is peritectic (Di + Pig = Fo + Liq).

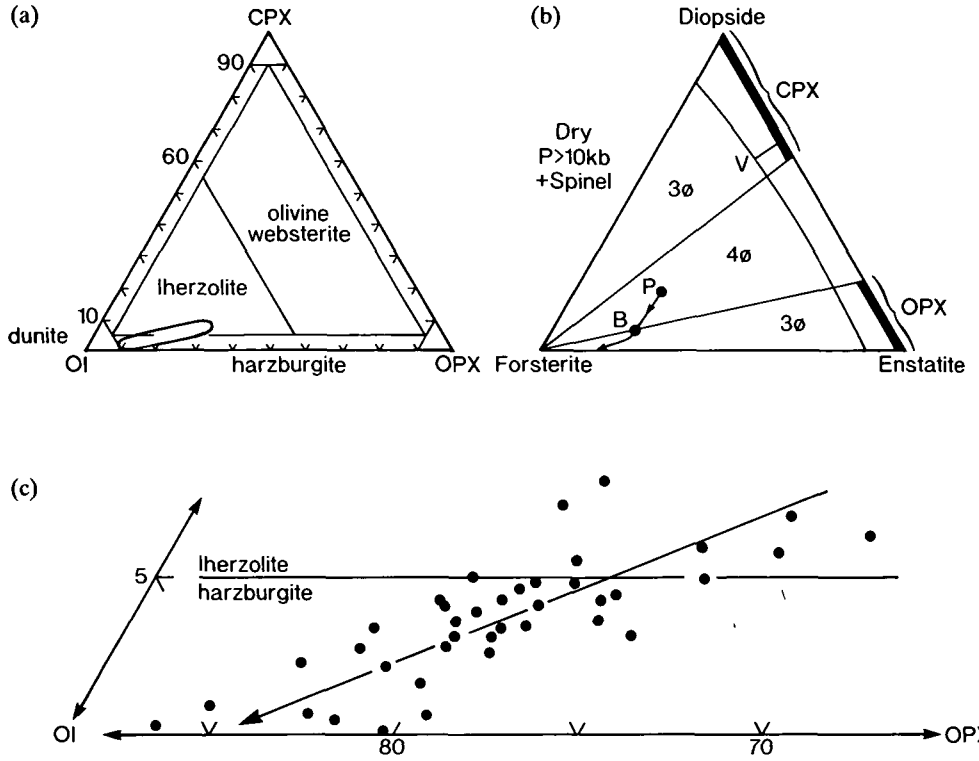

FIG. 7. (a) Modal ternary diagram Ol–Opx–Cpx with the compositions of abyssal peridotites from selected sites in the Atlantic, Pacific and Indian oceans (from Dick *et al.*, 1984). (b) Sketch of the synthetic system Di–Fo–En under anhydrous conditions at high pressures. Points P, B, and V correspond to those of Fig. 6. Melting relations in the three- and four-phase fields are discussed in the text (from Dick *et al.*, 1984, modified). (c) Expanded view of the base of (a), showing the compositional field for abyssal peridotites (from Dick *et al.*, 1984).

Whatever the pressure and type of melting, these initial liquids will not depart from either V or R until all Di is consumed. In the mean time, the solid will follow a path heading directly away from P, lying along lines passing either through V (finely dotted line VP) or R (thin solid line RP), here drawn as passing through R (path PA). Point A lies at the intersection of lines RP and FoG, where G represents that Pig composition saturated with Di and coexisting with liquid R, Di, and Fo. Application of the lever rule shows that Di melts out at ~7% melting and the residual peridotite A becomes $\sim Fo_{63}Pig_{37}$, or, in terms of starting components, $Fo_{63}En_{28}Di_9$. The disappearance of Di does not equate to the disappearance of Cpx from the source (as Pig is still present), but merely shows that the more fusible Cpx component will rapidly enter the melt and dominate its composition in the early melt fractions (see below). As soon as this component is released, Cpx will not be liable to melt so easily, as the steep slope of the Pig solidus indicates (Fig. 4a).

Further melting of peridotite A will yield liquids along RQ (Pig = Fo + Liq or Pig + Fo = Liq at higher pressures) and residues along AB. Path AB is slightly curved because of the continuously changing Pig composition, from Di-saturated at A to En-saturated at B. Point B lies at the intersection of lines QP and FoH, where H represents that Pig composition saturated with En and coexisting with liquid Q, En, and Fo. On its way to B, the solid path crosses the lherzolite/harzburgite boundary at ~16% melting. Application of the lever rule

shows that when the liquid arrives at Q, an additional 13% melt has been produced (i.e., 20% total melting) and the residue B has become $\sim Fo_{75}En_{23}Di_2$.

Point Q is peritectic where the remaining Pig will be consumed (Pig = Fo + En + Liq; but not at higher pressures) after ~2% melting (i.e., 22% total melting) leaving a residue C $\sim Fo_{77}En_{22}Di_1$. Peridotite C requires some 16% additional melting (i.e., 38% total melting) to exhaust its En content, in very good agreement with the experimentally derived Opx-out curve of Jaques & Green (1980). During this melting interval, the liquid composition moves along QK and the solid composition along the curved path CFo. The latter is curved to account for the continuously changing En composition, from Pig-saturated at J to Pig-free at En.

The point where the Di content of En disappears can be found by extrapolating line QPBC to its intersection with the Fo–En join at D (dot–dashed line CD). Application of the lever rule shows that an additional 4% melting is required until composition C loses all its Di, after which the residue D becomes $Fo_{82}En_{18}$ (cf. Fig. 7c, where the residual peridotite trend approaches asymptotically the olivine corner).

NON-LINEAR MELTING IN THE MANTLE: A NEW INTERPRETATION

The effects of solid solution

The mantle melting scenario developed above can be evaluated by means of equation (3), as the composition of successive residues and associated degrees of melting are all known from the phase diagram. The results of the present analysis are summarized in Table 2. Notwithstanding the negative olivine contribution to the melt, brought about by considering phase relations in the simplified CMS system at 1 atm which involve the peritectic dissolution of En, several important points are worth singling out. First of all, it seems impossible to model mantle melting accurately using only one set of ratios of phases entering the liquid; this corroborates the conclusions of Jaques & Green (1980) and Johan & Augé (1986) that mantle melting is primarily controlled by solid solution rather than eutectic behaviour. Melting proportions change whenever a phase reacts and/or disappears from a system, and depend heavily on the choice of the initial and final peridotite compositions. For

TABLE 2

Summary of spinel peridotite equilibrium melting in the Fo–En–Di system

Source	*Residue*	F(%)	*Fo*	*En*	*Di*	*Melting peridotite at low P*
P	A	7	2	13	85	FSL
A	C	15	−17	63	54	DSL + Cpx-bearing Hz*
C	D	4	−34	116	18	Cpx-saturated Hz
D	Fo	12	−50	150	—	Cpx-free Hz
A	D	19	−16	71	45	DSL + Cpx-bearing Hz* + Cpx-saturated Hz
P	C	22	−6	45	61	FSL + DSL + Cpx-bearing Hz*
P	D	26	−7	53	54	FSL + DSL + Cpx-bearing* + Cpx-saturated Hz
C	Fo	16	−41	137	4	Cpx-saturated Hz + Cpx-free Hz
P	DSL	11	2	20	78	FSL
DSL	DSH	13	−43	97	46	DSL + FSH
P	DSH	24	−15	57	58	FSL + DSL + FSH

* At high P, Cpx-saturated Hz will melt in addition to Cpx-bearing Hz.

Degrees of melting for the P–DSL and DSL–DSH intervals are from Michael & Bonatti (1985); that for the P–DSH interval is from Green *et al.* (1979).

example, for melting of fertile spinel lherzolites (path PA), the proportion of En in the melt would be significantly smaller than for melting of depleted spinel lherzolites and Cpx-bearing harzburgites (path AC). This is because the former melting episode takes place exclusively in the presence of free Di (Fig. 6), whereas the latter takes place exclusively in its absence, yet still in the presence of Cpx now in the form of Pig.

Mantle melting domains

In general, the proportion of Di in the melt decreases as the amount of Di in the system decreases, and the reverse is true for En. Careful examination of Table 2 reveals four distinct domains in the melting regime of upper-mantle peridotites. The first domain (PA) relates to melting of fertile spinel lherzolites where Di dominates the melt fraction. The second domain (AC) relates to the melting of depleted spinel lherzolites and Cpx-bearing harzburgites, in which En takes over while Di is still contributing a fair amount to the melt. The third domain (CD) relates to the melting of Cpx-saturated harzburgites where Di plays only a very subordinate role, and the fourth domain (DFo) relates to the melting of Cpx-free harzburgites where En reigns. However, the very good match between paths AC and AD suggests that the four domains above can be condensed to three, viz., PA, AD, and DFo, characterized by free Di, Di-saturated En, and Di-free En respectively. Inasmuch as path DFo is adequately accounted for by Fo–En equilibria, the problem reduces to establishing the phase melting proportions for paths PA and AD.

The paradoxical persistence of Cpx in melting residues

The suggested non-linearity in the mantle melting regime, which occurs at moderate Cpx levels (separating domains PA and AD above), is evident in a plot of modal wt.% Cpx vs. modal wt.% Ol abundances in abyssal and fertile peridotites (Fig. 8). {The six fertile spinel lherzolite compositions shown were chosen following the cosmochemical criteria for undepleted and slightly depleted upper-mantle peridotite described by Jagoutz *et al.* (1979) and Hart & Zindler (1986), and discussed by Kostopoulos & James (submitted). Particular attention was paid to exclude samples suspected of containing excess modal Cpx [see Stosch (1981), Preß *et al.* (1986), Song & Frey (1989), and Dick (1989), and additional references listed in Table 1]. Inclusion of such samples results in a compositional field for the fertile rocks that extends towards unrealistically high Cpx contents (i.e., 9–12 wt.%) at Ol levels clearly indicative of residual nature (i.e., 65–70 wt.%).} Although data for olivine contents between 60 and 65 wt.% are particularly scanty, perhaps because such relatively fertile peridotites would have always melted in oceanic environments, or remained deep enough during mantle flow not to be exposed by faulting, it is not possible that a linear extrapolation of the abyssal Ol–Cpx field will intersect the undepleted spinel lherzolite array. The two peridotite groups follow individual trends that meet at a point $\sim Ol_{64-65}Cpx_{7-6}$. This value is in excellent agreement with the calculated less refractory oceanic peridotite composition $Ol_{65}Opx_{28}Cpx_{6\cdot2}Sp_{0\cdot8}$ (Michael & Bonatti, 1985), and because it lies near the lherzolite/ harzburgite boundary (defined by 5 wt.% modal cpx) it is termed here depleted spinel lherzolite or DSL. This rock will be used as an endmember in both limbs of the dual melting regime (i.e., as endmember A in paths PA and AD).

The exact reason for the 'kink' in the melting proportions of Cpx within the lherzolite field is not known, but a possible explanation is offered below. It will be recalled that the disappearance of free Di from the Di–Fo–SiO_2 ternary (Fig. 6) was interpreted as the

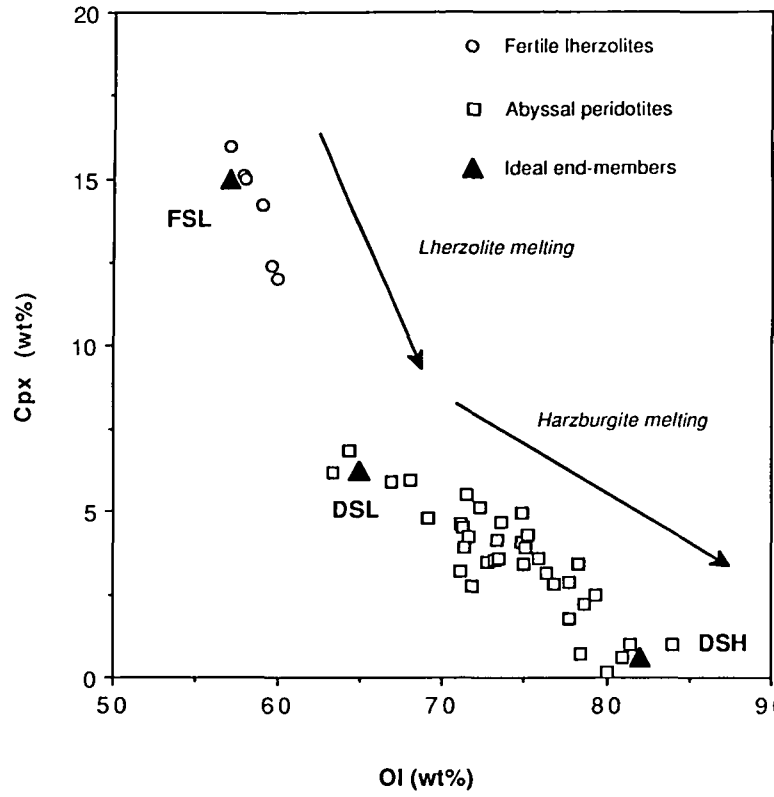

FIG. 8. Diagram of modal wt.% Cpx vs. modal wt.% Ol from abyssal Sp peridotites (data from Dick *et al.*, 1984; Michael & Bonatti, 1985; Dick, 1989) and fertile Sp lherzolite xenoliths of (near-)primitive upper-mantle composition (KLB-1: Takahashi, 1986; R717: Frey *et al.*, 1985; KH77-12: Roden *et al.*, 1988; RS1: Feigenson, 1986; Z-37: Bonatti *et al.*, 1986; GJ62.14: Furnes *et al.*, 1986*b*). Melting in the lherzolite facies is characterized by a much steeper slope compared with that in the harzburgite facies; this suggests an appreciably faster rate of Cpx consumption during the former melting episode. Calculated regression lines are: for the undepleted array: Cpx (wt.%) = 93·79 − 1·36 × Ol (wt.%); for the abyssal array: Cpx (wt.%) = 27·29 − 0·32 × Ol (wt.%). FSL, DSL, and DSH are discussed in the text.

disappearance of the most fusible Cpx component from the mantle. Cpx–Sp equilibria during mantle melting may be expressed as

$$\underset{\text{Spinel}}{MgAl_2O_4} + 2\ \underset{\text{Cr–CaTs}}{CaCrAlSiO_6} = \underset{\text{Picrochromite}}{MgCr_2O_4} + 2\ \underset{\text{CaTs}}{CaAlAlSiO_6}.$$

Thus, the afore-mentioned early-stage melting of Mg–Al-spinel by solid solution change to Cr-rich spinel will concomitantly 'accelerate' melting of Cpx by 'liberating' the fusible CaTs (Ca-Tschermak's) component. However, the solid solution transformation of spinel is accomplished rather rapidly, probably within 30 °C of the dry solidus (Jaques & Green, 1980). This is equivalent to ~4 kb of supra-solidus isentropic ascent, or, for a diapir with solidus-intersection conditions 1350 °C/18·5 kb, to ~8·5% melting (Kostopoulos & James, submitted). This inferred degree of melting agrees very well with the 7% estimate from the phase diagram and is consistent with the proposed mechanism.

Another interesting observation pertinent to the rate of consumption of Cpx in the upper mantle discussed herein comes from the modelling of the isotopic and rare-earth composi-

tion of MORB by Holness & Richter (1989). These workers concluded that the MORB source contains an enriched endmember that is uniformly dispersed in it and represents the first material to melt on decompression. The height above the solidus at which all the enriched endmember melts completely is ~12·5 km (Holness & Richter, 1989; fig. 8) by which point 7% melt has been released. These numbers compare directly with the depth and degree of melting respectively at which Di disappears from the model MORB mantle composition of Fig. 6 (point P) during melting.

With regard to the low-Cpx endmember of melting residues, the author employed a composition $Ol_{82}Opx_{17}Cpx_{0\cdot6}Sp_{0\cdot4}$, hereafter depleted spinel harzburgite or DSH, which is satisfactorily situated among the most depleted lithologies at the high-Ol end of the abyssal peridotite array (Fig. 8) and also, is in accord with the calculated average more refractory peridotite composition $Ol_{81}Opx_{19}Cpx_{0\cdot4}Sp_{0\cdot6}$ (Michael & Bonatti, 1985).

Melting coefficients for spinel lherzolites

Once the melting regime and endmember compositions of spinel peridotites have been established, the procedure of determining melt contribution coefficients can be outlined. The basic mass-balance equation that describes melting of a phase has the form (Shaw, 1970)

$$P_o = FP_l + (1-F)P_r \tag{6}$$

where P_o is the mass proportion of any phase in source, P_l is the mass proportion of the phase entering the melt, P_r is the mass proportion of the phase in the residue, and F is the degree of melting (mass proportion of liquid produced). Manipulation of (6) leads to

$$F = (P_o - P_r)/(P_l - P_r) \tag{7}$$

$$P_l = [P_o - (1-F)P_r]/F \tag{8}$$

$$P_r = (P_o - FP_l)/(1-F). \tag{9}$$

Equation (7) for olivine becomes

$$F = (Ol_o - Ol_r)/(Ol_l - Ol_r) \tag{10}$$

and for Opx

$$F = (Opx_o - Opx_r)/(Opx_l - Opx_r). \tag{11}$$

By eliminating F [i.e., by equating (10) and (11)], and assuming that

$$Opx_l/Ol_l = 6\cdot7 \tag{12}$$

(Cpx-free harzburgite eutectic; see discussion in the section on 'Melting of forsterite') the following equation is finally derived:

$$Ol_l = [Opx_r(Ol_o - Ol_r) - Ol_r(Opx_o - Opx_r)]/[6\cdot7(Ol_o - Ol_r) - (Opx_o - Opx_r)]. \tag{13}$$

Ol_l may be solved for using any two endmember peridotite compositions; it is then replaced in (10) to determine the degree of melting. Equation (8) is used next to derive the proportions of the other phases entering the melt. The technique was applied twice to evaluate melting coefficients in the lherzolite (FSL→DSL) and harzburgite (DSL→DSH) intervals separately. The resulting complete melting scheme is

FSL—12·5% (F)→DSL—23·5% (F)→DSH

Melting proportions are:

for the FSL–DSL interval: $Ol_{0.0121}Opx_{0.0806}Cpx_{0.7637}Sp_{0.1436}$;
for the DSL–DSH interval: $Ol_{0.0955}Opx_{0.6388}Cpx_{0.2447}Sp_{0.0210}$;
Cpx-free Sp harzburgite is melted in proportions $Ol_{0.1273}Opx_{0.8517}Sp_{0.0210}$;
(Cpx + Sp)-free harzburgite is melted in proportions $Ol_{0.13}Opx_{0.87}$.

The method presented here is arranged in such a way that the melting proportions of Ol + Opx and Cpx + Sp are treated by pairs. The rationale behind this is that the Ol + Opx pair controls the Si, Mg, Fe, and Ni content of the liquid, whereas the Cpx + Sp pair controls its Ca, Na, Cr, Ti, and Al content, thus providing internal consistency for the abundances of these elements. If, for example, the proportions of Ol and Cpx are changed in any endmember, the resulting change in the contribution of Ol to the liquid will induce a change in that of Opx, whereas the new Cpx melting coefficient will affect that of Sp.

Evaluation of Sp lherzolite melting models

The results of the present modelling are summarized in Table 3 and are plotted as Fig. 9. The results of the melting models of other workers (Table 1) are also plotted as Fig. 10. A comparison of Figs. 9 and 10 with Fig. 8 reveals the improved mantle melting scheme proposed in this manuscript in relation to earlier models. Variations in Ol and Cpx modal abundances have been successfully duplicated, and this holds true for Opx and Sp. Although (Cpx + Sp)-free residues of peridotite melting are very scarce, the present model simulates the modal mineralogies of recently reported, severely depleted harzburgites collected from the landward slopes of the Tonga Trench (Bloomer & Fisher, 1987) with surprising accuracy at all olivine levels. Using the calculated residual mantle compositions of Table 3 it is also possible to estimate the amount of excess modal clinopyroxene present in many peridotites [see Hart & Zindler (1986) and Kostopoulos & James (submitted) for details]. For example, addition of 4 wt.% Cpx (absolute amount) to the residue derived by 38% melting of a BSE Sp lherzolite source (Table 3) yields a composition $Ol_{77.4}Opx_{17.3}Cpx_{4.9}Sp_{0.4}$, that compares directly with sample DM1-7 of Song & Frey (1989) from Eastern China ($Ol_{77.4}Opx_{17.1}Cpx_{4.8}Sp_{0.7}$), for which macroscopic and chemical evidence is greatly in favour of excess modal Cpx.

Inspection of Tables 2 and 3 shows very good agreement in the melting coefficients of Ol, Opx, and Cpx for the FSL–DSL interval, as derived by the model developed here and the Di–Fo–SiO_2 system. Regarding the DSL–DSH interval, it can be seen that the negative contribution of Ol to the melt has been corrected but the melting coefficient of Cpx has become noticeably smaller. This is because no excess Cpx is now required to counterbalance the peritectically produced olivine in the ternary (i.e., Pig = Fo + Liq along RQ; Fig. 6). The low Cpx value reflects complex melting of CaTs-depleted Cr endiopside, partly in solid solution in Opx.

With respect to the melting models of other workers (Table 1) it can be seen from Fig. 10 that the Ottonello *et al.* (1984) and Dupuy *et al.* (1987) trends miss completely and widely both the undepleted lherzolite and abyssal peridotite arrays. All the other trends intersect the abyssal array at a specific point only and cannot satisfy the entire array. Moreover, most of them pass well outside the undepleted lherzolite array. Degrees of melting at which the various melting trends intersect the abyssal array also vary widely. Examples include: 10% (Roden *et al.*, 1988); 15% (Ewart & Hawkesworth, 1987); 20% (Beccaluva *et al.*, 1984); 25% (Pearce & Norry, 1979; Lippard *et al.*, 1986); 35% (Viereck *et al.*, 1989). Finally, many of the above trends fail to reproduce observed Opx contents (data from Dick *et al.*, 1984), yielding

TABLE 3

Modelling of melting residues

F (%)	*Calculated modal abundances (wt.%)* *Ol*	*Opx*	*Cpx*	*Sp*	*Reference compositions*
0	57·00	25·50	15·00	2·50	*Fertile spinel lherzolite (FSL) or Bulk Silicate Earth (BSE)*
1	57·56	25·68	14·38	2·38	*MORB–pyrolite (DMM)*
2	58·13	25·85	13·76	2·26	
3	58·70	26·03	13·13	2·14	
4	59·28	26·21	12·49	2·02	
5	59·86	26·40	11·85	1·89	
6	60·45	26·58	11·20	1·77	
7	61·05	26·77	10·55	1·64	Mt. Leura SL7 (Chen *et al.*, 1989)
8	61·65	26·95	9·89	1·51	
9	62·26	27·14	9·22	1·38	
10	62·87	27·34	8·54	1·25	
11	63·49	27·53	7·86	1·12	Hannuoba DM1-3 (Song & Frey, 1989)
12	64·12	27·73	7·17	0·99	
13	64·75	27·92	6·48	0·85	
13·4	65·00	28·00	6·20	0·80	*Depleted spinel lherzolite (DSL)*
14	65·34	27·79	6·09	0·79	
15	65·90	27·42	5·90	0·78	
16	66·47	27·06	5·71	0·76	
17	67·04	26·69	5·53	0·75	
18	67·62	26·31	5·34	0·74	
19	68·20	25·94	5·14	0·72	Lherzolite
20	68·79	25·55	4·95	0·71	Harzburgite
21	69·39	25·17	4·75	0·70	*Fertile spinel harzburgite (FSH)*
22	69·99	24·78	4·55	0·68	
23	70·60	24·39	4·35	0·67	***Cpx-bearing***
24	71·21	23·99	4·15	0·65	
25	71·83	23·59	3·95	0·64	
26	72·46	23·18	3·74	0·62	Average abyssal (Shibata & Thompson, 1986; Dick, 1989)
27	73·09	22·77	3·53	0·61	
28	73·73	22·36	3·32	0·59	Vanuatu 31564B (Barsdell & Smith, 1989)
29	74·37	21·94	3·11	0·58	
30	75·02	21·52	2·89	0·56	
31	75·68	21·09	2·68	0·55	
32	76·35	20·66	2·46	0·53	MAR 23°38′N, All96–10 (Dick *et al.*, 1984)
33	77·02	20·23	2·24	0·52	
34	77·70	19·79	2·01	0·50	MAR 23°38′N, All96-12 (Dick *et al.*, 1984)
35	78·38	19·35	1·79	0·48	
36	79·07	18·90	1·56	0·47	Av. Josephine (Dick, 1977)
37	79·77	18·45	1·33	0·45	
38	80·48	17·99	1·10	0·44	***Cpx-saturated***
39	81·19	17·53	0·86	0·42	
40	81·91	17·06	0·62	0·40	
40·1	81·99	17·02	0·60	0·40	*Depleted spinel harzburgite (DSH)*
41	82·64	16·59	0·38	0·39	
42	83·38	16·12	0·14	0·37	*Cpx-out*
43	84·10	15·55		0·35	
44	84·82	14·85		0·33	Oman 4091A (Brown, 1982)
45	85·54	14·14		0·31	
46	86·28	13·43		0·30	***Cpx-free***
47	87·01	12·71		0·28	Oman 4080A (Brown, 1982)
48	87·76	11·98		0·26	
49	88·52	11·24		0·24	
50	89·28	10·50		0·22	Tonga D88-AA-1 (Bloomer & Fisher, 1987)
51	90·05	9·75		0·20	
52	90·83	8·99		0·19	Oman 4167 (Brown, 1982)
53	91·61	8·22		0·17	

TABLE 3 (*Continued*)

Modelling of melting residues

F (%)	*Calculated modal abundances (wt.%)* *Ol*	*Opx*	*Cpx*	*Sp*	*Reference compositions*
54	92·40	7·45		0·15	SWIR 54°43'S, All-107-35 (Dick *et al.*, 1984)
55	93·21	6·67		0·13	Oman 2342 (Brown, 1982)
56	94·01	5·88		0·11	
57	94·83	5·08		0·09	Tonga D57-6A (Bloomer & Fisher, 1987)
58	95·66	4·28		0·07	
59	96·49	3·46		0·05	
60	97·33	2·64		0·03	*Sp-out*
61	98·18	1·81			
62	99·04	0·96			
63	99·90	0·10			*Opx-out*
63·2	100·00				

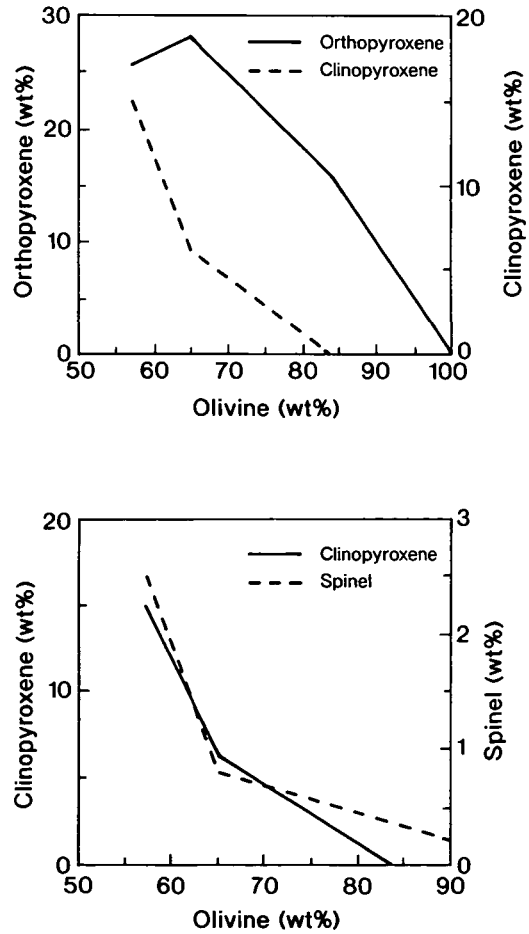

FIG. 9 (*Continued*)

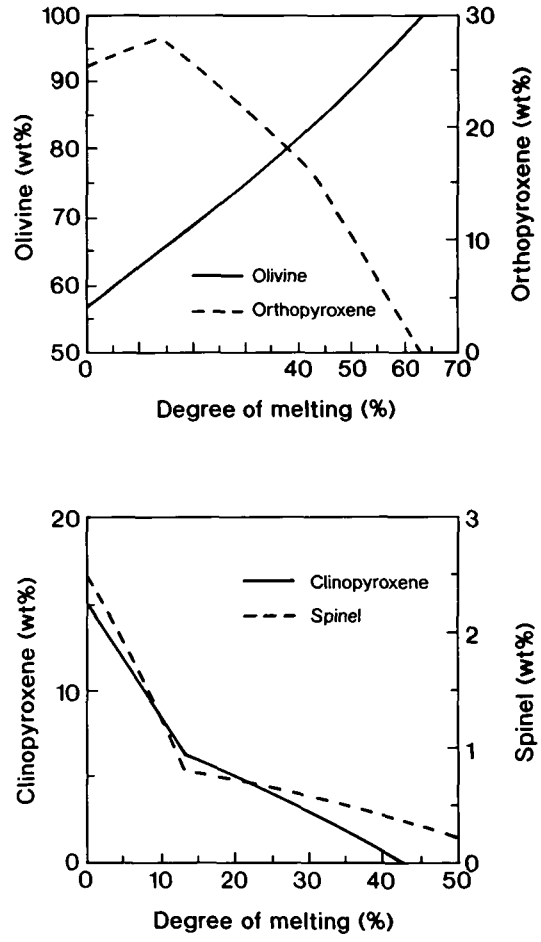

FIG. 9. Calculated modal wt.% mineralogies of melting peridotites as a function of the amount (wt.%) of residual Ol and the degree of partial melting. (See text and Table 3 for further details on the modelling.)

either exceptionally high values at moderate (i.e., 60–65%) Ol levels (e.g., Dupuy *et al.*, 1987; Viereck *et al.*, 1989), or yielding constant values throughout their melting histories (e.g., Lippard et al., 1986).

Melting in an adiabatically rising mantle

According to the present model, some 42% melting is required before Cpx disappears completely from a MORB–pyrolite mantle. Although this value is significantly higher than that suggested by the position of the Cpx-out curves determined by peridotite melting experiments (~22%; see Jaques & Green, 1980; Takahashi, 1986; McKenzie & Bickle, 1988), it must be emphasized that isobaric equilibrium melting is a gross oversimplification of the natural melting process and is not equivalent to melting during adiabatic upwelling. Thompson (1987) has also remarked that the concept of the depth of origin of magma in an adiabatically rising mantle casts doubt on the results of virtually all equilibrium melting experiments conducted so far, which have been used to identify the P–T conditions of basic magma genesis.

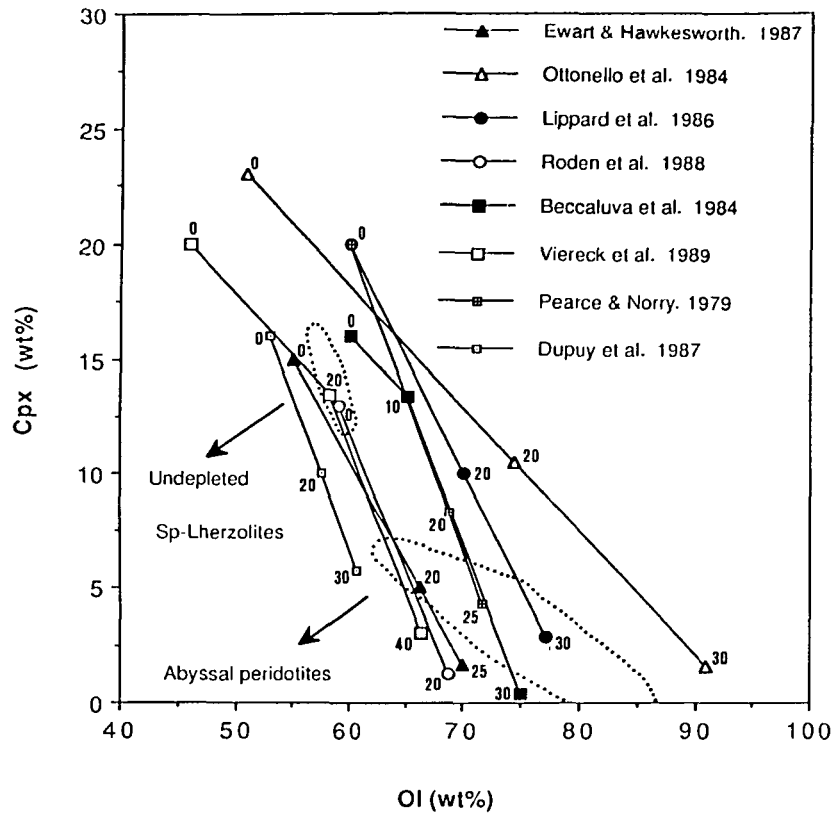

FIG. 10. Modal wt.% Cpx vs. modal wt.% Ol in residues of melting calculated using selected models from Table 1. Numbers next to symbols are wt.% melt. The undepleted lherzolite and abyssal peridotite arrays (follow arrows) are from Fig. 8. [Note the large uncertainty in positioning the starting fertile mantle composition and the inadequacy of the models to reproduce the abyssal array, as a result of maintaining phase melting proportions appropriate for lherzolite (i.e., Cpx-rich sources) only.]

Duncan & Green (1987) presented a refined three-stage melting history of upper-mantle spinel peridotite (see also Green *et al.*, 1979; Duncan & Green, 1980). First-stage melting (~24%) of adiabatically rising MORB–pyrolite produces picritic MORB which segregates between 80- and 50-km depth (24–15 kb). The residue from this melting episode is harzburgite, which re-equilibrates to spinel lherzolite at lower pressures and temperatures as a result of unmixing of aluminous orthopyroxene (2·5 wt.% CaO). Second-stage melting (~10%) of the residual diapir at some shallower depth (10–12 kb; 33–40 km) produces magnesian olivine tholeiites and a more depleted harzburgite or lherzolite residue (carrying moderately aluminous pyroxenes; 2–4 wt.% Al_2O_3), which may continue its upwelling until emplaced at the base of oceanic crust. If second-stage melting occurs at even shallower depths (~25 km; 7·5 kb) the lavas produced are magnesian quartz tholeiites and the residues are extremely depleted harzburgites (carrying low-Al pyroxenes; ~1 wt.% Al_2O_3), similar to the harzburgite tectonites seen at the base of some ophiolites. Third-stage melting (< 10% ?) of the above residues in the presence of H_2O-rich fluids in a tensional environment under a strongly adiabatic thermal gradient may lead to formation of boninites (Cape Vogel type).

Although stemming from isobaric equilibrium melting experiments, the message from Duncan & Green's (1987) work is clear: harzburgites belonging to supra-subduction-zone ophiolites have experienced some 35% melting, yet they contain traces of low-Al Cpx. The truth of this conclusion has been reiterated by Falloon *et al.* (1988), who recognized that incremental melting of upwelling MORB–pyrolite with continuous removal of melt requires an appreciable shift of the Cpx-out curve in residual compositions to significantly higher degrees of melting than are possible under equilibrium conditions. Bonatti & Michael (1989) have also estimated degrees of depletion in the sub-oceanic mantle relative to pyrolite, ranging from ~ 10 to $\sim 25\%$ in abyssal peridotites to $> 30\%$ in subduction-related peridotites.

It is clear then that the commonly postulated disappearance of Cpx from BSE and DMM compositions at $\sim 22\%$ melting is greatly in error if melting in a rising mantle diapir is considered. Inaccurate modelling of Cpx is potentially significant for elements such as Si, Mg, Fe, Al, Cr, Ni, and Co, and can be of major significance for Na, Ca, Sc, V, Ti, and the REE as this mineral typically carries $> 75\%$ of a Sp lherzolite's (and more than 95% of a Sp harzburgite's) budget of these elements. The early disappearance of Cpx from melting residues, invoked by various workers (Table 1), exhausts the concentrations of the elements hosted in this phase at lower melt fractions. This explains the use of higher than BSE wt.% modal Cpx or transition- and rare-earth-element concentrations in the starting source composition in their models, as well as many unsuccessful attempts to simulate the abundances of transition elements (especially Ti, V, and Sc) in MORB and arc magmas.

It should be emphasized here that the proposed melting scheme applies only to residual upper-mantle peridotite compositions. Most magmas represent accumulations (i.e., pooled melts) of individual melt fractions (i.e., instantaneous melts), each fraction having been in equilibrium with a unique mantle composition in the melting column during adiabatic rise. Therefore, degrees of melting inferred from trace-element abundances in magmas cannot be equated to the degree of melting undergone by their parental material. Kostopoulos & James (submitted) have, for example, calculated that the total melt extraction beneath mid-ocean ridges underlain by mantle with normal potential temperature (i.e., $T_{pot} = 1280\,^{\circ}C$) reaches 22%, whereas the pooled melts (i.e., N-MORB) represent integrated melt removal of the order of 12%. Dredged abyssal peridotites contain ~ 4 wt.% Cpx on average (Dick *et al.*, 1984; Dick, 1989), implying maximum degrees of melting underneath spreading centres near 24%, in excellent agreement with the results of the present modelling. Further details on the vertical compositional stratification of the oceanic lithosphere (i.e., harzburgite top→lherzolite bottom) and solidus equations for selected depleted upper-mantle compositions are presented elsewhere (Kostopoulos & James, submitted).

CONCLUSIONS

Detailed examination of liquidus phase relationships in binary and ternary joins of the CFMAS+Cr system has allowed a rigorous determination of the dry melting path of an initially fertile spinel peridotite composition resembling Bulk Silicate Earth or MORB–pyrolite. It is demonstrated that it is impossible to model mantle melting accurately using only one set of ratios of phases entering the melt; this implies that the melting process is primarily controlled by solid solution rather than eutectic behaviour. The proportions of phases entering a melt depend on whether a phase reacts and/or disappears from a system, and on the choice of the initial and final peridotite compositions. Four discrete domains in the melting regime of upper-mantle peridotites are distinguished, each

characterized by different phase melting coefficients, relating to the melting of: (1) lherzolites, (2) clinopyroxene-bearing harzburgites (i.e., free-clinopyroxene), (3) clinopyroxene-saturated harzburgites (i.e., clinopyroxene in solid solution in orthopyroxene), and (4) clinopyroxene-free harzburgites (i.e., no clinopyroxene). The proposed non-linear fashion in which mantle lithologies melt explains the inadequacy of all previous models to reproduce the observed compositions of upper-mantle peridotite melting residues. It is suggested that: (1) olivine and orthopyroxene will melt cotectically; (2) clinopyroxene and spinel will lose most of their aluminous component after ~8% melting within the first 4 kb (~12 km) of ascent from the dry solidus; and (3) clinopyroxene will disappear completely from a MORB–pyrolite mantle after ~42% melting. Although such a number is significantly higher than that dictated by the position of the clinopyroxene-out curves from peridotite isobaric equilibrium melting experiments (~22%), it is emphasized that the latter are a gross oversimplification of the natural melting process and are not equivalent to melting during adiabatic upwelling. It is concluded that the commonly postulated disappearance of clinopyroxene from fertile peridotite compositions at ~22% melting is greatly in error if melting in an adiabatically rising mantle is considered, thus providing an explanation for many unsuccessful attempts by various authors to model the behaviour of transition elements in sub-oceanic and supra-subduction-zone mantle and derivative magmas.

ACKNOWLEDGEMENTS

Perusals by Julian Pearce, Joe Cann, Martin Flower, and Dave Latin are greatly appreciated. Karen Atkinson drew the diagrams.

REFERENCES

Arai, S., 1987. An estimation of the least depleted spinel peridotite on the basis of olivine–spinel mantle array. *Neues Jahrb. Miner. Mh.* **8**, 347–54.

Arculus, R. J., Gillberg, M. E., & Osborn, E. F., 1974. The system MgO–iron oxide–Cr_2O_3–SiO_2: phase relations among olivine, pyroxene, silica and spinel in air at 1 atm. *Yb. Carnegie Inst. Wash.* **73**, 317–22.

—— Osborn, E. F., 1975. Phase relations in the system MgO–iron oxide–Cr_2O_3–SiO_2. *Ibid.* **74**, 507–12.

Augé, T., 1983. Étude minéralogique et pétrographique de roches basiques et ultrabasiques du complexe ophiolitique du Nord Oman. *Doc. B.R.G.M.* **65**, 263 pp.

Barsdell, M., & Smith, I. E. M., 1989. Petrology of recrystallized ultramafic xenoliths from Merelava volcano, Vanuatu. *Contr. Miner. Petrol.* **102**, 230–41.

Beccaluva, L., Ohnenstetter, D., Ohnenstetter, M., & Paupy, A., 1984. Two magmatic series with island arc affinities within the Vourinos ophiolite. *Ibid.* **85**, 253–71.

Bloomer, S. H., & Fisher, R. L., 1987. Petrology and geochemistry of igneous rocks from the Tonga Trench—a non-accreting plate boundary. *J. Geol.* **95**, 469–95.

Bodinier, J. L., 1988. Geochemistry and petrogenesis of the Lanzo peridotite body, Western Alps. *Tectonophysics* **149**, 67–88.

Bonatti, E., & Michael, P. J., 1989. Mantle peridotites from continental rifts to ocean basins to subduction zones. *Earth Planet. Sci. Lett.* **91**, 297–311.

—— Ottonello, G., & Hamlyn, P. R., 1986. Peridotites from the island of Zabargad (St. John), Red Sea: petrology and geochemistry. *J. Geophys. Res.* **91**, 599–631.

Bowen, N. L., & Andersen, O., 1914. The binary system MgO–SiO_2. *Am. J. Sci.* **37**, 487–500.

Boyd, F. R., England, J. L., & Davis, B. T. C., 1964. Effects of pressure on the melting and polymorphism of enstatite, $MgSiO_3$. *J. Geophys. Res.* **69**, 2101–9.

Brophy, J. G., & Marsh, B. D., 1986. On the origin of high-alumina arc-basalt and the mechanics of melt extraction. *J. Petrology* **27**, 763–89.

Brown, M. A., 1982. Chromite deposits and their ultramafic host rocks in the Oman ophiolite. Unpublished Ph.D. Thesis, Open University, 263 pp.

Carlson, W. D., 1988. Subsolidus phase equilibria on the forsterite-saturated join $Mg_2Si_2O_6$–$CaMgSi_2O_6$ at atmospheric pressure. *Am. Miner.* **73**, 232–41.

—— Lindsley, D. H., 1988. Thermochemistry of pyroxenes on the join $Mg_2Si_2O_6$–$CaMgSi_2O_6$. *Ibid.* **73**, 242–52.

Carter, J. L., 1970. Mineralogy and chemistry of the Earth's upper mantle based on the partial fusion–partial crystallization model. *Geol. Soc. Am. Bull.* **81**, 2021–34.

Chen, C. H., & Presnall, D. C., 1975. The system Mg_2SiO_4–SiO_2 at pressures up to 25 kilobars. *Am. Miner.* **60**,

398–406.
Chen, C. -Y., Frey, F. A., & Song, A., 1989. Evolution of the upper mantle beneath southeast Australia: geochemical evidence from peridotite xenoliths in Mount Leura basanite. *Earth Planet. Sci. Lett.* **93**, 195–209.
Condie, K. C. 1985. Secular variation in the composition of basalts: an index to mantle evolution. *J. Petrology* **26**, 545–63.
Davidson, P. M., & Lindsley, D. H., 1985. Thermodynamic analysis of quadrilateral pyroxenes. Part II. Model calibration from experiments and applications to geothermometry. *Contr. Miner. Petrol.* **91**, 390–404.
Dick, H. J. B., 1977. Partial melting in the Josephine peridotite 1. The effect on mineral composition and its consequence for geobarometry and geothermometry. *Am. J. Sci.* **277**, 801–32.
—— 1989. Abyssal peridotites, very slow spreading ridges and ocean ridge magmatism. In: Saunders, A. D., & Norry, M. J. (eds.) *Magmatism in the Ocean Basins. Geol. Soc. Lond., Spec. Publ.* **42**, 71–105.
—— Bullen, T., 1984. Chromian spinel as a petrogenetic indicator in abyssal and alpine-type peridotites and spatially associated lavas. *Contr. Miner. Petrol.* **86**, 54–76.
—— Fisher, R. L., 1984. Mineralogic studies of the residues of mantle melting: abyssal and alpine-type peridotites. In: Kornprobst, J. (ed.) *Kimberlites II: The Mantle and Crust–Mantle Relationships. Developments in Petrology*, 11B. Amsterdam: Elsevier, 295–308.
—— —— Bryan, W. L., 1984. Mineralogic variability of the uppermost mantle along mid-ocean ridges. *Earth Planet. Sci. Lett.* **69**, 88–106.
Dickey, J. S., Yoder, H. S., Jr., & Schairer, J. F., 1971. Chromium in silicate–oxide systems. *Yb. Carnegie Inst. Wash.* **70**, 118–22.
Dobson, P. F., & O'Neil, J. R., 1987. Stable isotope compositions and water contents of boninite series volcanic rocks from Chichi-jima, Bonin islands, Japan. *Earth Planet. Sci. Lett.* **82**, 75–86.
Duncan, R. A., & Green, D. H., 1980. Role of multistage melting in the formation of oceanic crust. *Geology* **8**, 22–6.
—— —— 1987. The genesis of refractory melts in the formation of oceanic crust. *Contr. Miner. Petrol.* **96**, 326–42.
Dupuy, C., Dostal, J., & Bodinier, J. L., 1987. Geochemistry of spinel peridotite inclusions in basalts from Sardinia. *Miner. Mag.* **51**, 561–8.
Eggler, D. H., 1987. Discussion of recent papers on carbonated peridotite, bearing on mantle metasomatism and magmatism: an alternative. *Earth Planet. Sci. Lett.* **82**, 398–400.
Elthorn, D. L., 1989. Pressure of origin of primary mid-ocean ridge basalts. In: Saunders, A. D., & Norry, M. J. (eds.) *Magmatism in the Ocean Basins. Geol. Soc. Lond., Spec. Publ.* **42**, 125–36.
Ewart, A., & Hawkesworth, C. J., 1987. The Pleistocene–Recent Tonga–Kermadec arc lavas: interpretation of new isotopic and rare earth data in terms of a depleted mantle source model. *J. Petrology* **28**, 495–530.
Falloon, T. J., & Green, D. H., 1988. Anhydrous partial melting of peridotite from 8 to 35 kb and the petrogenesis of MORB. *J. Petrology, Special Lithosphere Issue* 379–414.
—— —— Hatton, C. J., & Harris, K. L., 1988. Anhydrous partial melting of a fertile and depleted peridotite from 2 to 30 kb and application to basalt petrogenesis. *J. Petrology* **29**, 1257–82.
Feigenson, M. D., 1986. Continental alkali basalts as mixtures of kimberlite and depleted mantle: evidence from Kilbourne Hole Maar, New Mexico. *Geophys. Res. Lett.* **13**, 965–8.
Frey, F. A., 1984. Rare earth element abundances in upper mantle rocks. In: Henderson, P. (ed.) *Rare Earth Element Geochemistry. Developments in Geochemistry*, 2. Amsterdam: Elsevier, 153–203.
—— Suen, C. J., & Stockman, H. W., 1985. The Ronda high-temperature peridotite: geochemistry and petrogenesis. *Geochim. Cosmochim. Acta* **49**, 2469–91.
Furnes, H., Brekke, H., Nordas, J., & Hertogen, J., 1986*a*. Lower Palaeozoic convergent plate margin volcanism on Bømlo, southwest Norwegian Caledonides: geochemistry and petrogenesis. *Geol. Mag.* **123**, 123–42.
—— Pedersen, R. B., & Maaløe, S., 1986*b*. Petrology and geochemistry of spinel peridotite nodules and host basalt, Vestspitsbergen. *Norsk Geol. Tidsskr.* **66**, 53–68.
—— Vad, E., Austrheim, H., Mitchell, J. G., & Garmann, L. B., 1987. Geochemistry of basalt lavas from the Vetfjella and adjacent areas, Dronning Maud Land, Antarctica. *Lithos* **20**, 337–56.
Green, D. H., 1976. Experimental testing of 'equilibrium' partial melting of peridotite under water-saturated, high-pressure conditions. *Can. Miner.* **14**, 255–68.
—— Hibberson, W. O., & Jaques, A. L., 1979. Petrogenesis of mid-ocean ridge basalts. In: McElhinny, M. W. (ed.) *The Earth: Its Origin, Structure and Evolution.* New York: Academic Press, 265–99.
—— Pearson, N. J., 1985. Rare earth element partitioning between clinopyroxene and silicate liquid at moderate to high pressure. *Contr. Miner. Petrol.* **91**, 24–36.
Grutzeck, M., Kridelbaugh, S., & Weill, D., 1974. The distribution of Sr and REE between diopside and silicate liquid. *Geophys. Res. Lett.* **1**, 273–5.
Hart, S. R., & Zindler, A., 1986. In search of a bulk earth composition. *Chem. Geol.* **57**, 247–67.
Holness, M. B., & Richter, F. M., 1989. Possible effects of spreading rate on MORB isotopic and rare earth composition arising from melting of a heterogeneous source. *J. Geol.* **97**, 247–60.
Huebner, S., 1980. Pyroxene phase equilibria at low pressure. In: Prewitt, C. T. (ed.) *Pyroxenes. Miner. Soc. Am., Rev. Miner.* **7**, 213–88.
Irvine, T. N., 1977. Chromite crystallization in the join Mg_2SiO_4–$CaMgSi_2O_6$–$CaAl_2Si_2O_8$–$MgCr_2O_4$–SiO_2. *Yb. Carnegie Inst. Wash.* **76**, 465–72.
—— Sharpe, M. R., 1986. Magma mixing and the origin of stratiform oxide ore zones in the Bushveld and Stillwater Complexes. In: Gallagher, M. J., Ixer, R. A., Neary, C. R., & Pritchard, H. M. (eds.) *Metallogeny of Basic and Ultrabasic Rocks.* London: Inst. Min. Metal., 183–98.

Jagoutz, E., Palme, H., Baddenhausen, H., Blum, K., Cendales, M., Dreibus, G., Spettel, B., Lorenz, V., & Wänke, H., 1979. The abundances of major, minor and trace elements in the earth's mantle as derived from primitive ultramafic nodules. *Proc. Lunar Planet. Sci. Conf.* **10,** 2031–50.

Jaques, A. L., & Green, D. H., 1980. Anhydrous melting of peridotite at 0–15 kb pressure and the genesis of tholeiitic basalts. *Contr. Miner. Petrol.* **73,** 287–310.

Johan, J., & Augé, T., 1986. Ophiolitic mantle sequences and their evolution: mineral chemistry constraints. In: Gallagher, M. J., Ixer, R. A., Neary, C. R., & Pritchard, H. M. (eds.) *Metallogeny of Basic and Ultrabasic Rocks.* London: Inst. Min. Metal., 305–17.

Kato, T., & Kumazawa, M., 1985. Effect of high pressure on the melting relation in the system Mg_2SiO_4–$MgSiO_3$ Part I: Eutectic relation up to 7 GPa. *Miner. Abstr.* **38,** 453–4.

Klein, E. M., & Langmuir, C. H., 1987. Global correlations of ocean ridge basalt chemistry with axial depth and crustal thickness. *J. Geophys. Res.* **92,** 8089–115.

Kostopoulos, D. K., & James, S. D., submitted. The nature, composition and melting regime of the upper mantle and the influence of variably stretched lithosphere on magma production and trace element geochemistry. *J. Petrology.*

Kushiro, I., 1969. The system forsterite–diopside–silica with and without water at high pressures. *Am. J. Sci.,* Schairer vol. **267-A,** 269–94.

—— Yoder, H. S., & Nishikawa, M., 1968. Effect of water on the melting of enstatite. *Geol. Soc. Am. Bull.* **79,** 1685–92.

Kyser, T. K., Cameron, W. E., & Nisbet, E. G., 1986. Boninite petrogenesis and alteration history: constraints from stable isotope compositions of boninites from Cape Vogel, New Caledonia and Cyprus. *Contr. Miner. Petrol.* **93,** 222–6.

Leeman, W. P., 1976. Petrogenesis of McKinney (Snake River) olivine tholeiite in light of rare-earth and Cr/Ni distributions. *Geol. Soc. Am. Bull.* **87,** 1582–6.

Lin, P. N., Stern, R. J., & Bloomer, S. H., 1989. Shoshonitic volcanism in the northern Mariana arc 2. Large-ion lithophile and rare-earth element abundances: evidence for the source of incompatible element enrichments in intraoceanic arcs. *J. Geophys. Res.* **94,** 4497–514.

Lindsley, D. H., & Andersen, D. J., 1983. A two-pyroxene thermometer. *Ibid.* **88,** Suppl., A887–A906.

Lippard, S. J., Shelton, A. W., & Gass, I. G., 1986. The ophiolite of Northern Oman. *Mem. Geol. Soc. Lond.* **11,** 178 pp.

McKay, G. A., Wagstaff, J., & Yang, S.-R., 1986. Clinopyroxene REE distribution coefficients for shergottites: the REE content of the Shergotty melt. *Geochim. Cosmochim. Acta* **50,** 927–37.

McKenzie, D. P., 1984. The generation and compaction of partially molten rock. *J. Petrology* **25,** 713–65.

—— 1985. The extraction of magma from the crust and mantle. *Earth Planet. Sci. Lett.* **74,** 81–91.

—— Bickle, M. J., 1988. The volume and composition of melt generated by extension of the lithosphere. *J. Petrology* **29,** 625–79.

Michael, P. J., 1988. The concentration, behavior and storage of H_2O in the suboceanic upper mantle: implications for mantle metasomatism. *Geochim. Cosmochim. Acta* **52,** 555–66.

—— Bonatti, E., 1985. Peridotite composition from the North Atlantic: regional and tectonic variations and implications for partial melting. *Earth Planet. Sci. Lett.* **73,** 91–104.

—— Chase, R. L., 1987. The influence of primary magma composition, H_2O and pressure on mid-ocean ridge basalt differentiation. *Contr. Miner. Petrol.* **96,** 245–63.

Morse, S. A., 1980. *Basalts and Phase Diagrams.* Heidelberg: Springer-Verlag, 493 pp.

Muan, A., 1975. Phase relations in chromium oxide-containing systems at elevated temperatures. *Geochim. Cosmochim. Acta* **39,** 791–802.

Nakamura, N., Unruh, D. M., Tatsumoto, M., & Hutchison, R., 1982. Origin and evolution of the Nakhla meteorite inferred from the Sm–Nd and U–Pb systematics and REE, Ba, Sr, Rb and K abundances. *Ibid.* **46,** 1555–73.

Navon, O., & Stolper, E., 1987. Geochemical consequences of melt percolation: the upper mantle as a chromatographic column. *J. Geol.* **95,** 285–307.

Nicholls, I. A., 1974. Liquids in equilibrium with peridotitic mineral assemblages at high water pressures. *Contr. Miner. Petrol.* **45,** 289–316.

—— Ringwood, A. E., 1972. Production of silica-saturated tholeiitic magmas in island arcs. *Earth Planet. Sci. Lett.* **17,** 243–6.

—— —— 1973. Effect of water on olivine stability in tholeiites and the production of silica-saturated magmas in the island arc environment. *J. Geol.* **81,** 285–300.

Onuma, K., 1983. Phase relations in the Cr-poor part of the system diopside–anorthite–forsterite–$MgCr_2O_4$ in air at 1 atm. *J. Fac. Sci., Hokkaido Univ.,* Ser. IV **20,** 171–94.

—— Tohara, T., 1983. Effect of chromium on phase relations in the join forsterite–anorthite–diopside in air at 1 atm. *Contr. Miner. Petrol.* **84,** 174–81.

Ottonello, G., Ernst, W. G., & Joron, J. L., 1984. Rare earth and 3d transition element geochemistry of peridotitic rocks: 1: Peridotites from the western Alps. *J. Petrology* **25,** 343–72.

Pearce, J. A., & Norry, M. J., 1979. Petrogenetic implications of Ti, Zr, Y and Nb variations in volcanic rocks. *Contr. Miner. Petrol.* **69,** 33–47.

Presnall, D. C., Dixon, J. R., O'Donnell, T. H., & Dixon, S. A., 1979. Generation of mid-ocean ridge tholeiites. *J. Petrology* **20,** 3–35.

Preß, S., Witt, G., Seck, H. A., Eonov, D., & Kovalenko, V. I., 1986. Spinel peridotite xenoliths from the Tariat depression, Mongolia. I: Major element chemistry and mineralogy of a primitive mantle xenolith suite. *Geochim. Cosmochim. Acta* **50,** 2587–99.

Prinzhofer, A., & Allègre, C. J., 1985. Residual peridotites and the mechanisms of partial melting. *Earth Planet. Sci. Lett.* **74,** 251–65.

Ribe, N. M., 1985. The generation and composition of partial melts in the earth's mantle. *Ibid.* **73,** 361–76.

—— 1988. Dynamical geochemistry of the Hawaiian plume. *Ibid.* **88,** 37–46.

Roberts, S., 1986. The role of igneous processes in the formation of ophiolitic chromitite. Unpublished Ph.D. Thesis, Open University, 261 pp.

Roden, M. F., Irving, A. J., & Murthy, V. R., 1988. Isotopic and trace element composition of the upper mantle beneath a young continental rift: results from Killbourne Hole, New Mexico. *Geochim. Cosmochim. Acta* **52,** 461–73.

Shaw, D. M., 1970. Trace element fractionation during anatexis. *Ibid.* **34,** 237–43.

Shibata, T., & Thompson, G., 1986. Peridotites from the mid-Atlantic ridge at 43 °N and their petrogenetic relation to abyssal tholeiites. *Contr. Miner. Petrol.* **93,** 144–59.

Sinigoi, S., Comin-Chiaramonti, P., & Alberti, A. A., 1980. Phase relations in the partial melting of the Baldissero spinel-lherzolite (Ivrea–Verbano Zone, Western Alps, Italy). *Ibid.* **75,** 111–21.

Song, Y., & Frey, F. A., 1989. Geochemistry of peridotite xenoliths from Hannuoba, Eastern China: implications for subcontinental mantle heterogeneity. *Geochim. Cosmochim. Acta* **53,** 97–113.

Stosch, H. G., 1981. Sc, Cr, Co and Ni partitioning between minerals from spinel peridotite xenoliths. *Contr. Miner. Petrol.* **78,** 166–74.

—— Lugmair, G. W., & Kovalenko, V. I., 1986. Spinel peridotite xenoliths from the Tariat depression, Mongolia. II: Geochemistry and Nd and Sr isotopic composition and their implications for the evolution of the subcontinental lithosphere. *Geochim. Cosmochim. Acta* **50,** 2601–14.

Takahashi, E., 1986. Melting of a dry peridotite KLB-1 up to 14 GPa: implications on the origin of peridotitic upper mantle. *J. Geophys. Res.* **91,** 9367–82.

Thompson, R. N., 1987. Phase-equilibria constraints on the genesis and magmatic evolution of oceanic basalts. *Earth-Sci. Rev.* **24,** 161–210.

—— Morrison, M. A., Hendry, G. L., & Parry, S. J., 1984. An assessment of the relative roles of crust and mantle in magma genesis: an elemental approach. *Phil. Trans. R. Soc. Lond.* **A310,** 549–90.

Van der Laan, S. R., Flower, M. F. J., & Koster van Groos, A. F., 1989. Experimental evidence for the origin of boninites: near liquidus phase relations to 7·5 kbar. In: Crawford, A. J. (ed.) *Boninites*. London: Unwin–Hyman, 112–47.

Viereck, L. G., Flower, M. F. J., Hertogen, J., Schmincke, H. U., & Jenner, G. A., 1989. The genesis and significance of N-MORB sub-types. *Contr. Miner. Petrol.* **102,** 112–26.

Vukadinovic, D., & Nicholls, I. A., 1989. The petrogenesis of island arc basalts from Gunung Slamet volcano, Indonesia: trace element and $^{87}Sr/^{86}Sr$ constraints. *Geochim. Cosmochim. Acta* **53,** 2349–63.

Walker, D. A., & Cameron, W. E., 1983. Boninite primary magmas: evidence from the Cape Vogel Peninsula, PNG. *Contr. Miner. Petrol.* **83,** 150–8.

Walker, J. A., 1984. Volcanic rocks from the Nejapa and Granada cinder cone alignments, Nicaragua, central America. *J. Petrology* **25,** 299–342.

White, W. M., & Schilling, J.-G., 1978. The nature and origin of geochemical variation in Mid-Atlantic Ridge basalts from the central North Atlantic. *Geochim. Cosmochim. Acta* **42,** 1501–16.

Wood, D. A., 1978. Major and trace element variations in the Tertiary lavas of eastern Iceland and their significance with respect to the Iceland geochemical anomaly. *J. Petrology* **19,** 393–436.

—— 1979. Dynamic partial melting: its application to the petrogenesis of basalts erupted in Iceland, the Faeroe Islands, the Isle of Skye (Scotland) and the Troodos massif (Cyprus). *Geochim. Cosmochim. Acta* **43,** 1031–46.

Wyllie, P. J., 1987. Discussion of recent papers on carbonated peridotite, bearing on mantle metasomatism and magmatism. *Earth Planet. Sci. Lett.* **82,** 391–7.

—— 1988. Magma genesis, plate tectonics, and chemical differentiation of the Earth. *Rev. Geophys.* **26,** 370–404.